Scientific Reports

https://doi.org/10.1038/s41598-026-44561-x

Article in Press

# Isobaric quantitative proteomics reveals altered extracellular matrix, cytoskeletal, and degradation pathways in glaucomatous trabecular meshwork cells

Received: 19 August 2025

Accepted: 12 March 2026

Published online: 18 March 2026

Cite this article as: Holden P., Sun Y.Y., Zientek K. *et al.* Isobaric quantitative proteomics reveals altered extracellular matrix, cytoskeletal, and degradation pathways in glaucomatous trabecular meshwork cells. *Sci Rep* (2026). https://doi.org/10.1038/s41598-026-44561-x

**Paul Holden, Ying Ying Sun, Keith Zientek, Phillip A. Wilmarth, Ashok P. Reddy & Kate E. Keller**

# Isobaric Quantitative Proteomics Reveals Altered Extracellular Matrix, Cytoskeletal, and Degradation Pathways in Glaucomatous Trabecular Meshwork Cells

Paul Holden[1], Ying Ying Sun[1], Keith Zientek[2] , Phillip A. Wilmarth[2], Ashok P. Reddy[2], and Kate E. Keller[1,*]

[1]Casey Eye Institute, Oregon Health & Science University, 3181 SW Sam Jackson Park Road, Portland OR 97239 USA.

[2]Proteomics Shared Resources, Oregon Health & Science University, 3181 SW Sam Jackson Park Road, Portland OR 97239 USA.

[*]To whom correspondence should be addressed: gregorka@ohsu.edu

**Running title:** TMT labeling of glaucomatous trabecular meshwork cells.

**Keywords:** trabecular meshwork, glaucoma, tandem mass tags, proteomics

**Abstract**

Glaucoma trabecular meshwork (GTM) cells cultured *in vitro* retain many characteristics of their *in situ* phenotype. Here, we used isobaric tandem mass tags (TMTpro) to label peptides from glaucomatous and non-glaucomatous TM (NTM) cells to identify differentially regulated proteins. Confluent NTM (n=5) and GTM (n=5) cells were lysed, proteins were trypsin digested, and peptides were labeled with 18-plex TMTpro. TMT-labeled peptides were fractionated on an Orbitrap Fusion mass spectrometer and data were processed using the PAW/Comet pipeline and EdgeR with Benjami-Hochberg multiple correction testing. Isobaric multiplexed quantitative proteomics identified 206 proteins that were significantly (FDR<0.1) upregulated in GTM cells, 42 proteins that were downregulated, with 5270 non-candidates. Significant regulated pathways included extracellular matrix (DCN, COL4A1, CHI3L1), Wnt signaling (FZD1, FZD7, GSK3B), cytoskeletal regulation (ROCK2, MSN, TPM2, VIM, NF2), protein degradation (USP9X, LAMP1, SYNV1, UBE2L3), and nuclear proteins (LMNA, DFFA, CHMP3, RAD21). Western immunoblotting studies confirmed the TMTpro data. Immunofluorescence showed that the SNX7-stained nucleoli of GTM cells were significantly ($p<0.05$) larger, and the DIAPH2 immunostaining was more distended into the cytosol than in NTM cells. This study identified many significantly regulated proteins in cultured GTM cells, and the results revealed several new avenues for developing clinical therapies for glaucoma patients.

## Introduction

Glaucoma is an eye disease that affect millions of individuals worldwide[1]. The most common form is primary open-angle glaucoma (POAG), which is associated with elevated intraocular pressure (IOP) and causes progressive axon degeneration in the optic nerve. In healthy adults, the mean IOP is kept in a narrow range between 15-16 mmHg due to a balance between aqueous humor (AH) fluid formation by the ciliary body and drainage from the anterior chamber[2]. The main drainage route is through the trabecular meshwork (TM) tissue[3]. The precise synthesis and organization of extracellular matrix (ECM) molecules in the TM aids fluid egress. If IOP starts to increase, a homeostatic response, where TM cells activate matrix metalloproteinases to remodel the ECM, allows greater outflow and lowers IOP[2]. In the glaucomatous TM, there is an accumulation of disorganized ECM and fewer TM cells, which show increased actin stress fibers and contractility than age-matched non-glaucomatous tissue[4-6]. These features compromise the ability of TM cells to regulate outflow and homeostatically adjust IOP. A sustained IOP above 20 mmHg is a significant risk factor for development of POAG.

A major limitation for investigating the molecular profiles of glaucoma TM is that the tissue is relatively small and there are fewer TM cells than age-matched controls[6]. In addition, glaucoma eyes are not as readily available from eye biobanks as their healthy donor counterparts, which has limited transcriptomic and proteomic studies on glaucomatous TM. To overcome this, primary TM cells cultured from healthy and glaucomatous TM tissue are increasingly used as a model to study disease[7-10]. Primary cells are known to retain molecular expression patterns of the tissues from which they are derived[11,12]. Similarly, the expression levels of certain molecules are similar between glaucomatous TM cells and tissues e.g. increased expression of α-smooth muscle actin (α-SMA)[13-15]. Using cultured cells, numerous studies have identified genes, proteins, and phenotypic differences between glaucomatous and age-matched healthy TM cells[9,15-18]. Thus, cells cultured from glaucomatous TM tissue are an important resource to investigate this disease.

Liquid chromatography-Mass Spectrometry (LC-MS) studies have identified the proteomic profiles of normal or glaucomatous TM tissue[19,20], cultured TGFβ-treated TM cells[21], the transformed glaucomatous cell strain GTM3[22], dexamethasone-treated

or mechanically stretched human TM cells[23,24], human aqueous humor (AH)[25,26], glaucomatous AH[27], and extracellular vesicles derived from conditioned media of cultured normal or glaucomatous TM cells[28,29]. Chip-based antibody arrays have also investigated differential protein levels between age and sex-matched normal and POAG TM tissue[30]. Newer technology and reagents in the proteomics field have increased detection and accuracy. Isobaric labeling accuracy has been addressed by newer Orbitrap instrument advances where synchronous precursor selection MS3 scans are used to generate the reporter ion signals[31]. In addition, newer tandem mass tag reagents (TMTpro) have expanded the multiplexing capacity to 18 channels in a single plex[32,33]. Using these advances, proteins in segmental outflow TM tissues have been analyzed[34] and the protein profiles of dexamethasone-induced ocular hypertensive rats[35] were investigated. Yet, multiplexed TMT proteomics has not yet been used to study glaucomatous TM.

A better understanding of the molecular profiles of healthy and POAG TM is needed to design novel IOP-lowering therapies for glaucoma patients. In the current study, we used 18-plex TMTpro isobaric labeling quantitative advances to compare proteome profiles from cultured non-glaucomatous (NTM) and glaucomatous (GTM) cell samples to a depth of 5,500 proteins. A total of 248 proteins had significant relative abundance differences in GTM cells. Pathway analysis identified ECM/cell adhesion, Wnt signaling, the cytoskeleton, protein degradation and nuclear proteins as significantly regulated pathways. The results presented here reveal several new avenues for developing clinical therapies for glaucoma patients.



## Results

A total of 20 primary trabecular meshwork cell strains were used in this study (biological replicates; Table 1). Ten cell strains were from non-glaucomatous human donor eyes, while 10 cell strains were from those with an ocular history of glaucoma. These cell strains were age-, race-, and sex-matched. For the TMTpro analysis in this study, we chose a subset of n=5 NTM and n=5 GTM cell strains that were age, race, and sex-matched and that were wild-type for myocilin missense mutations.

**Table 1. Demographics of human donor eyes used in this study**. Glaucoma status is shown, as well as medications (if known). POAG = primary open-angle glaucoma. Cell strains were used for TMTpro proteomics (TMT), Western immunoblot (WB), and/or immunofluorescence (IF) assays.

| Cell strain | Age | Sex | Cause of Death | Glaucoma (medication) | Experiment | Sample key |
|---|---|---|---|---|---|---|
| 2021-1493 | 74 | F | Subdural bleed | No | TMT; WB | N-wt-12 |
| 2022-0794 | 80 | M | Respiratory failure | No | TMT; WB | N-wt-1 |
| 2022-0140 | 77 | F | Cardiogenic shock | No | TMT; WB | N-hom-2 |
| 2022-0791 | 59 | M | Mantle cell lymphoma | No | TMT; WB | N-hom-6 |
| 2022-1032 | 71 | F | Natural causes | No | TMT; WB | N-wt-16 |
| 2020-0984 | 69 | M | Advanced Parkinson's and dementia | No | IF | n/a |
| 2021-1110 | 77 | F | Lung cancer | No | WB; IF | n/a |
| 2022-0707 | 78 | F | Respiratory failure | No | WB; IF | n/a |
| 2023-0775 | 86 | M | Vfib arrest | No | WB | n/a |
| 2023-0747 | 76 | M | Natural causes | No | WB | n/a |
| | | | | | | |
| 2019-1757 | 92 | F | Cardiogenic shock | POAG (latanoprost) | TMT; WB | G-wt-9 |
| 2022-0949 | 61 | F | Pneumonia | POAG | TMT; WB | G-wt-17 |
| 2022-1033 | 78 | M | Cardiac arrest | POAG | TMT; WB | G-wt-15 |
| 2018-1672 | 57 | M | Respiratory failure | Glaucoma | TMT; WB | G-wt-5 |
| 2019-1150 | 81 | F | Breast cancer | POAG (combigan) | TMT; WB | G-hom-13 |
| 2021-0034 | 70 | M | Heart failure | POAG | WB | n/a |
| 2021-1912 | 73 | F | Myocardial infarction | Glaucoma | IF | n/a |
| 2022-1058 | 93 | F | Acute respiratory failure | Glaucoma | IF | n/a |
| 2024-1471 | 81 | M | Cardiac arrest | Glaucoma | WB | n/a |
| 2024-1491 | 82 | M | Intracerebral hemorrhage | Glaucoma | WB | n/a |

Trypsin-digested proteins from NTM (n=5) and GTM (n=5) cell layers were labeled with 18-plex TMTpro reagents and separated by LC-MS. Following stringent data analysis, peptides from a total of 5518 proteins were detected (Supplemental Table S3). Of these, a total of 248 proteins were differentially regulated between GTM and NTM cells with 206 proteins significantly upregulated in glaucoma samples, and 42 proteins significantly downregulated with a false discovery rate (FDR) <0.1 after multiple-testing corrections. Table 2 lists the top 20 upregulated and downregulated proteins. The full list of differentially regulated proteins can be found in Supplemental Table S4. Fifty-seven upregulated proteins had a log2FC > 1.0 (2-fold change), while eight downregulated proteins had a log2FC < -1.0 (-2-fold change). Interestingly, the TMT counts of 18 upregulated proteins listed in Table 2 were at background levels in NTM cells (highlighted orange, Supplemental Table S4). These 18 proteins are clustered in the top left area of the MA plot (Figure 1A). Of these 18 proteins, 8 proteins (44%) were associated with the nucleus/nucleoplasm and 6 (33%) were cytoskeletal proteins.



**Table 2:** Top 20 up- and down-regulated (gray) differentially abundant proteins in GTM cells compared to NTM cells (FDR<0.1). LogFC is the log fold-change, FDR is the false discovery rate.

| Protein Name | Accession | Fold Change (FC) | logFC | P-value | FDR |
|---|---|---|---|---|---|
| CNOT11 | Q9UKZ1 | 241.969 | 7.918 | 0.000002 | 0.000363 |
| SNX7 | Q9UNH6 | 86.862 | 6.440 | 0.000002 | 0.000408 |
| CAMSAP1 | Q5T5Y3 | 71.950 | 6.168 | 0.000014 | 0.001330 |
| AVEN | Q9NQS1 | 64.520 | 6.011 | 0.000001 | 0.000288 |
| LMNA | P02545 | 53.160 | 5.731 | 0.000003 | 0.000456 |
| USP9X | Q93008 | 44.015 | 5.459 | 0.000001 | 0.000229 |
| ROCK2 | O75116 | 34.171 | 5.094 | 0.000002 | 0.000408 |
| PBXIP1 | Q96AQ6 | 31.610 | 4.981 | 0.000004 | 0.000514 |
| CCDC9 | Q9Y3X0 | 29.044 | 4.860 | 0.000005 | 0.000615 |
| SF3A2 | Q15428 | 28.482 | 4.831 | 0.000000 | 0.000101 |
| PYM1 | Q9BRP8 | 26.879 | 4.747 | 0.000002 | 0.000362 |
| STK24 | Q9Y6E0 | 25.130 | 4.650 | 0.000002 | 0.000362 |
| SHPK | Q9UHJ6 | 23.622 | 4.561 | 0.000032 | 0.002631 |
| DERL2 | Q9GZP9 | 20.282 | 4.341 | 0.000003 | 0.000484 |
| SH3BP2 | P78314 | 18.274 | 4.191 | 0.000004 | 0.000496 |
| MSN | P26038 | 15.760 | 3.977 | 0.000001 | 0.000267 |
| TPM2 | P07951 | 14.710 | 3.878 | 0.000007 | 0.000807 |

| | | | | | |
|---|---|---|---|---|---|
| TERF2 | Q15554 | 14.657 | 3.872 | 0.000013 | 0.001273 |
| MMGT1 | Q8N4V1 | 14.245 | 3.832 | 0.000003 | 0.000462 |
| RFC3 | P40938 | 14.024 | 3.810 | 0.000001 | 0.000288 |
| ANXA1 | P04083 | -1.483 | -0.568 | 0.002491 | 0.065476 |
| RRP8 | O43159 | -1.525 | -0.609 | 0.000142 | 0.007441 |
| SEPTIN8 | Q92599 | -1.634 | -0.708 | 0.000162 | 0.008339 |
| HSPA14 | Q0VDF9 | -1.644 | -0.717 | 0.002926 | 0.073732 |
| MALT1 | Q9UDY8 | -1.670 | -0.740 | 0.000126 | 0.006852 |
| ATP2B4 | P23634 | -1.688 | -0.755 | 0.001017 | 0.034864 |
| NANS | Q9NR45 | -1.741 | -0.800 | 0.002434 | 0.064889 |
| TMTC1 | Q8IUR5 | -1.744 | -0.802 | 0.000414 | 0.017568 |
| MME | P08473 | -1.756 | -0.812 | 0.003155 | 0.078074 |
| SNRNP40 | Q96DI7 | -1.783 | -0.834 | 0.002326 | 0.062619 |
| FAF2 | Q96CS3 | -1.785 | -0.836 | 0.000853 | 0.030470 |
| SLC29A1 | Q99808 | -1.950 | -0.964 | 0.000183 | 0.009084 |
| SLC30A7 | Q8NEW0 | -2.021 | -1.015 | 0.000301 | 0.013727 |
| METTL2B | Q6P1Q9 | -2.225 | -1.154 | 0.000067 | 0.004400 |
| ANXA11 | P50995 | -2.345 | -1.230 | 0.000076 | 0.004766 |
| DNAJC16 | Q9Y2G8 | -3.304 | -1.724 | 0.004169 | 0.095972 |
| CALU | O43852 | -3.460 | -1.791 | 0.004284 | 0.096176 |
| CYBRD1 | Q53TN4 | -3.511 | -1.812 | 0.000001 | 0.000218 |
| SEC61A1 | P61619 | -3.550 | -1.828 | 0.002924 | 0.073732 |
| TBCB | Q99426 | -3.860 | -1.949 | 0.002301 | 0.062229 |

An MA plot shows the up- (red) and downregulated (blue) proteins compared to the non-candidates (black) (Figure 1A). Interconnected pathways identified by STRING of all 206 upregulated and 42 downregulated proteins are shown (Figure 1B, C). Gene ontology (GO) pathway analysis was also performed. The top 20 GO:Biological processes featured organelle organization, catabolic processes, protein localization, and negative regulation of nuclease activity (Figure 2A), while those for GO:Cellular Component pathways included endopeptidase complex, endoplasmic reticulum-containing complex, focal adhesions, lysosomes and extracellular vesicles (Figure 2B). Five pathways were identified for GO:Molecular Function, which were RNA binding, cytoskeletal protein binding, and ribonucleoprotein complex binding (Figure 2C). Each of the proteins in the significant high level GO categories for each of the pathways are listed in Supplemental Table 5.

**Figure 1**

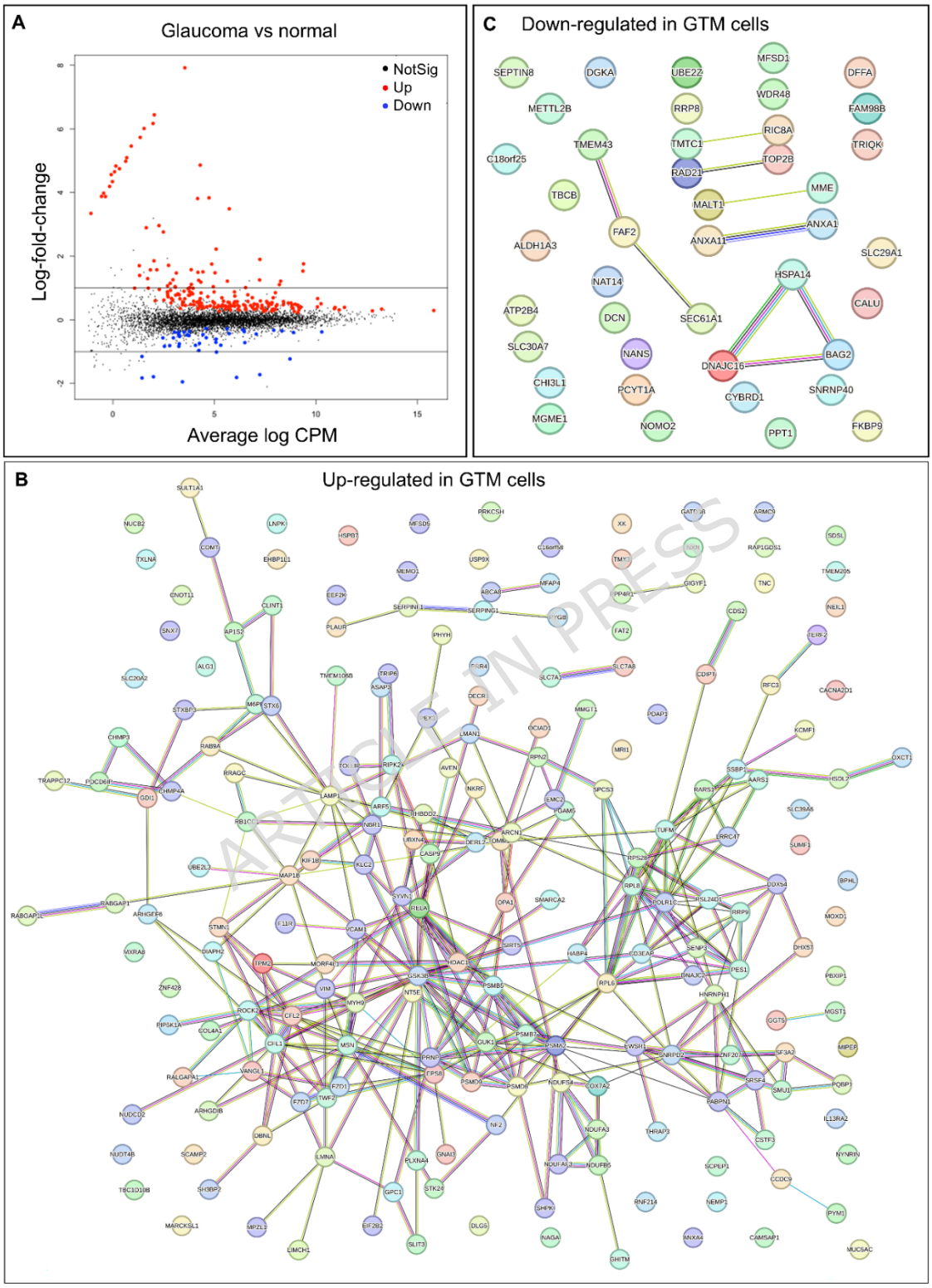


**Figure 1. String interaction network analysis and MA plot.** (A) MA plot showing the up- (red; n=206) and downregulated (blue; n=42) proteins in GTM cells compared

to the non-candidates (black; n=5270). The two solid horizontal lines are the 2-fold change lines. (B) All 206 significantly (FDR<0.1) upregulated proteins in GTM cells were entered into STRING and network analysis is shown. All proteins are represented by a node (circle). Those that have known interactions are connected by straight lines. (C) STRING network analysis of all 42 significantly (FDR<0.1) downregulated proteins in GTM cells. Colored nodes = query proteins and first shell of interactors. Known interactions: cyan = from curated databases, pink = experimentally determined. Predicted interactions: green = gene neighborhood, red = gene fusions, blue=gene co-occurrence. Others: khaki = text mining, black = co-expression, lavender = protein homology.

**Figure 2**

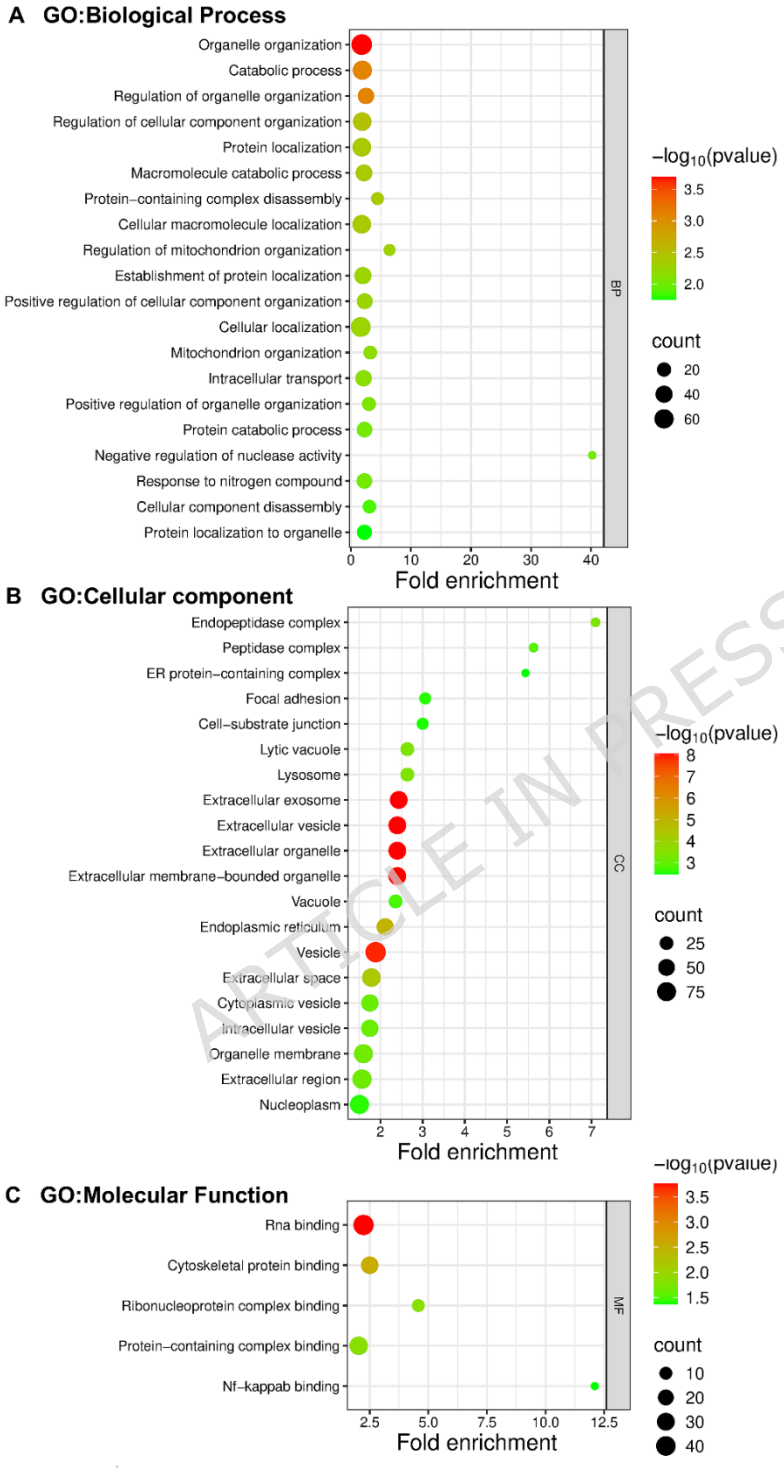


**Figure 2. GO pathways identified by enrichment analysis.** All 248 differentially abundant proteins were analyzed. The top 20 pathways for (A) GO:Biological process and (B) GO:cellular component are shown. (C) All five pathways enriched for

GO:molecular function are shown. Individual proteins in each high-level GO category can be found in Supplemental Table 5.

Next, we sought to validate the TMT proteomic data using Western immunoblots and performed a more in-depth analysis of some of the significantly regulated pathways. To simplify, we focused on four cellular compartments: the extracellular and cell membrane, cytoskeletal proteins, proteins involved in protein degradation pathways, and nuclear proteins. Proteins selected for more in-depth analysis were based on prior association with glaucoma, trabecular cell function, and/or the TMTpro fold changes.

Several ECM proteins showed significant differences between GTM and NTM cells. These included the upregulation of GPC1 (1.7-fold), MFAP4 (1.5-fold), HABP (1.3-fold), COL4A1 (1.3-fold) and TNC (1.3-fold), and the downregulation of DCN (-1.35-fold) and CHI3L1 (-1.2-fold). Decorin (DCN) is involved in collagen fibrillogenesis and growth factor regulation and is associated with glaucoma [36]. Western immunoblot analysis showed decreased protein levels of decorin in conditioned media (Figure 3A). Also, arresten, the proteolytically cleaved non-collagenous 1 (NC1) domain of the basement membrane collagen type IV, alpha 1 chain (COL4A1) [37], was more abundant in GTM cells. In addition to differential regulation of ECM proteins, several cell adhesion and transmembrane receptors were altered. These included upregulation of VCAM1 (1.3-fold), FAT2 (1.3-fold), and JAM1 (1.2-fold). Western immunoblotting confirmed the upregulation of Frizzled-1 (FZD1; 1.3-fold in TMT data), a receptor for Wnt signaling, in GTM cells (Figure 3B). Other Wnt pathway proteins were also upregulated in GTM cells including FZD7 and GSKbeta, which were upregulated 2.8- and 1.3-fold, respectively (Supplemental Table S4). Differentially abundant TMT-labeled proteins in the Wnt pathway are shown in Figure 3C.

Figure 3

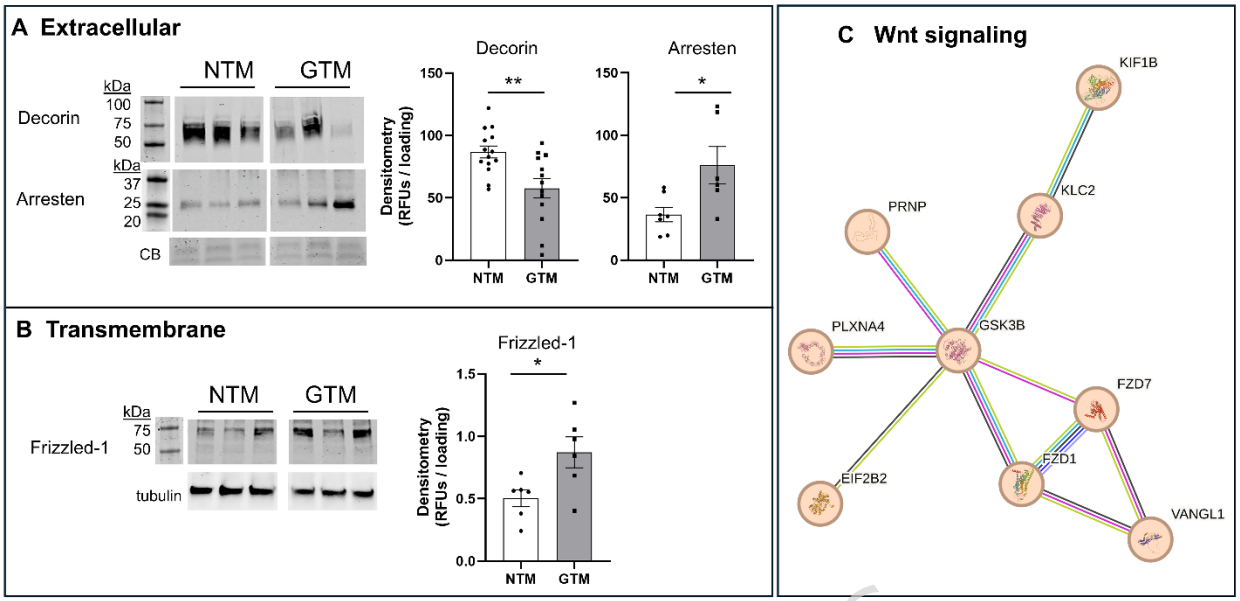


**Figure 3. Western immunoblot and densitometry of selected extracellular matrix and cell membrane proteins.** (A) Decorin (DCN) is significantly downregulated in conditioned media from GTM cells. Arresten, the proteolytically cleaved non-collagenous 1 (NC1) domain of collagen type IV, alpha 1 chain (COL4A1), is significantly upregulated in conditioned media from GTM cells. (B) The Wnt receptor protein, Frizzled-1 (FZD1), is significantly upregulated in GTM cell lysates. Representative Western immunoblots show 3x NTM and 3x GTM cell strains, which are cropped from different parts of the same membranes. Original blots are presented in the Supplementary File. Densitometric quantitation is from n=14 biological replicates for decorin, n=7 for arresten, and n=6 for frizzled-1. Coomassie blue (CB) stained gels or tubulin were used for loading control normalization. *p<0.05; **p<0.01. (C) Nine proteins in the Wnt pathway were significantly regulated in GTM cells as depicted by STRING network analysis. Known interactions: cyan = from curated databases, pink = experimentally determined. Predicted interactions: blue=gene co-occurrence. Others: khaki = text mining, black = co-expression, lavender = protein homology. Filled nodes: a 3D structure is known or predicted.

Next, we investigated the cytoskeleton and associated proteins because there are increased stress fibers and contractility in GTM cells[5,38]. Moesin (MSN) and merlin (NF2) are proteins that anchor actin filaments to plasma membranes[39,40]. Thus, they play important roles in cell shape, filopodia, cell-cell recognition and signal transduction. MSN was upregulated 15-fold in GTM cells (Table 2), while NF2 was upregulated 1.4-fold (Supplementary Table S4). MSN showed significant upregulation by Western immunoblot (Figure 4A). Tropomyosin beta (TPM2) binds along the length

of actin filaments, which allows it to stabilize the filament and regulate the interactions of other actin-binding proteins[41]. TPM2 was upregulated 14.7-fold by TMTpro and was significantly increased by Western immunoblot (Figure 4A). Cofilins (CFL1 and CFL2) are actin-binding proteins that bind to filamentous F-actin and sever the filament, aiding its depolymerization[42]. These proteins were upregulated in GTM cells (CFL1, 1.4-fold; CFL2, 3.3-fold) (Table 2 and Supplemental Table S4). Rho-associated protein kinase 2 (ROCK2) is a key regulator of actin stress fibers and formation of focal adhesions[43]. ROCK2 was upregulated 34-fold in GTM cells (Table 2) and upregulated in Western immunoblot (Figure 4A). Differentially abundant tubulin-associated proteins included upregulation of STMN1 (1.2-fold) and downregulation of TBCB (-3.9-fold). The intermediate filament protein vimentin (VIM) functions to position and anchor organelles in the cytosol of the cells and maintains cell integrity. It is upregulated when cells undergo EMT, and we previously showed the *VIM* gene to be upregulated in GTM cells[15]. Thus, it was not surprising to find that VIM protein was upregulated 1.4-fold in TMTpro data (Supplemental Table S4) and by Western immunoblotting (Figure 4A). STRING interaction network analysis showed that eight significantly regulated proteins were involved in actin depolymerization in GTM cells (Figure 4B). The actin-binding formin, DIAPH2, was upregulated 1.4-fold in GTM cells (Supplemental Table S4). When cells were immunostained, we found that DIAPH2 localized to perinuclear region in NTM cells (Figure 4C), and that DIAPH2 immunostaining distended into the cytosol in GTM cells. Surprisingly, DIAPH2 did not colocalize with the actin cytoskeleton in either NTM or GTM cells. Together, these data provide further evidence that the cytoskeleton of GTM cells is dysfunctional.

Figure 4

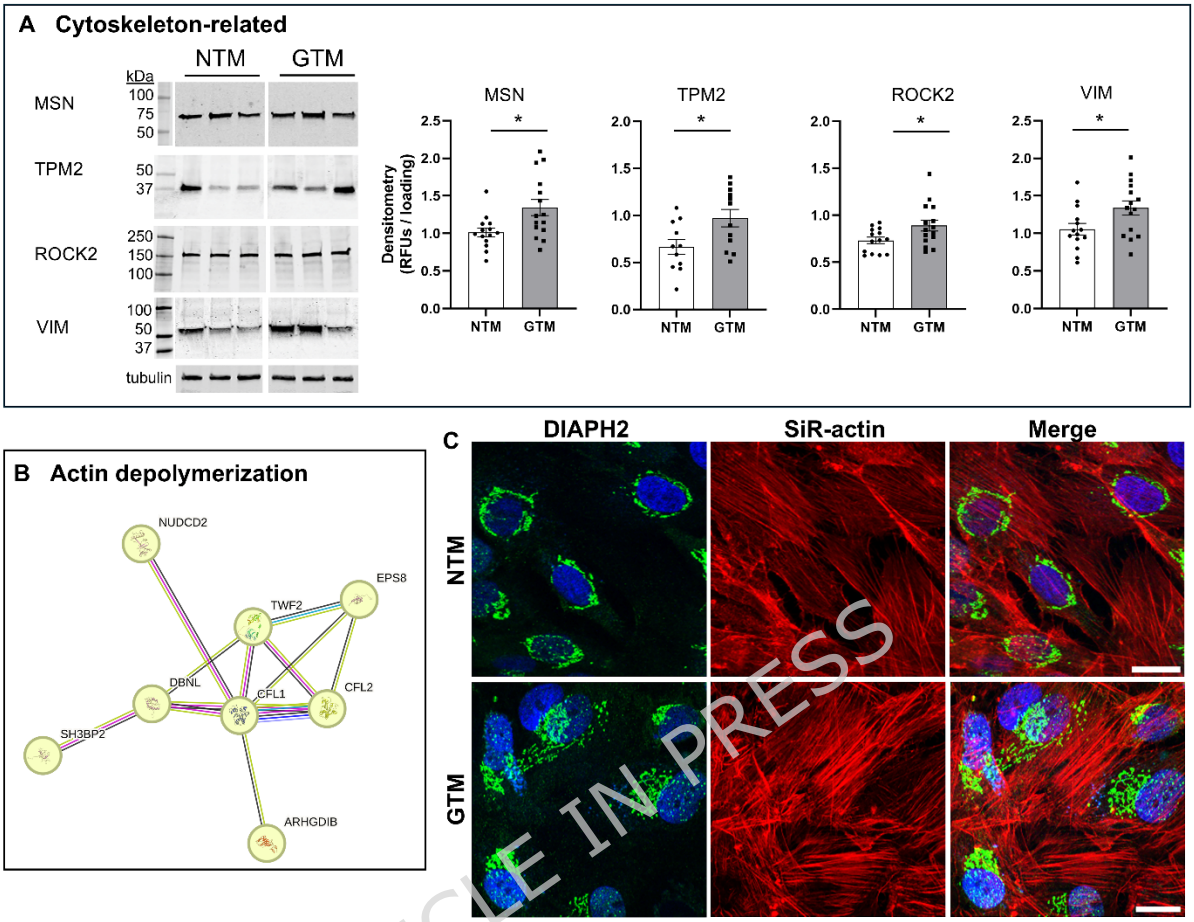


**Figure 4. Western immunoblot and densitometry of selected cytoskeletal-related proteins.** (A) The actin-binding proteins moesin (MSN), tropomyosin-2 (TPM2), and Rho-associated coiled-coil containing protein kinase 2 (ROCK2) are significantly upregulated in GTM cell lysates. The intermediate filament protein, vimentin (VIM), is also significantly upregulated in GTM cell lysates. Representative Western immunoblots show 3x NTM and 3x GTM cell strains. Original blots are presented in the Supplementary File. Densitometric quantitation is from n=15 biological replicates for MSN, n=11 for TPM2, n=14 for ROCK2, and n=14 for VIM. Tubulin was used for loading control normalization. *p<0.05. (B) Eight proteins involved with actin depolymerization were significantly regulated in GTM cells as depicted by STRING network analysis. Known interactions: cyan = from curated databases, pink = experimentally determined. Predicted interactions: green = gene neighborhood, blue=gene co-occurrence. Others: khaki = text mining, black = co-expression, lavender = protein homology. Filled nodes: a 3D structure is known or predicted. (C) The formin, DIAPH2, localized to the perinuclear region in NTM cells. In GTM cells, the DIAPH2 immunostaining was more distended from the perinuclear region. There was no colocalization with SiR-actin (red) in either NTM or GTM cells. Nuclei are stained with DAPI. Scale bar = 20 µm.

Pathway analysis showed that various pathways involved in catabolic processes were significantly affected in GTM cells. Two main catabolic pathways for degrading cellular materials in TM cells are the ubiquitin-proteasome system (UPS) and the autophagy-lysosomal (AL) pathways[44,45]. Our TMTpro proteomic data showed upregulation of several ubiquitin (Ub) E2 and E3 enzymes, which tag proteins with Ub therefore identifying them for degradation. These included UBE2L3 (1.6-fold), SYVN1 (1.4-fold), and KCMF1 (1.4-fold) (Supplemental Table S4). However, other enzymes involved in the UPS pathway had opposite effects. For instance, UBE2Z was downregulated -1.48-fold. Also, the ubiquitin hydrolase, USP9X, which removes ubiquitin from proteins, was upregulated 44-fold (Table 2), which was confirmed by Western immunoblotting (Figure 5A). Proteins in the AL pathway are also affected. LAMP1, which plays an important role in lysosome function, is upregulated 3.4-fold in GTM cells by TMTpro (Supplemental Table S4 and by Western immunoblotting (Figure 5A). When all significantly regulated proteins were entered into STRING, 16 proteins were identified to be involved in autophagy (Figure 5B). Together, these data suggest that protein degradation pathways are compromised and cellular homeostasis in GTM cells is disrupted.

**Figure 5**

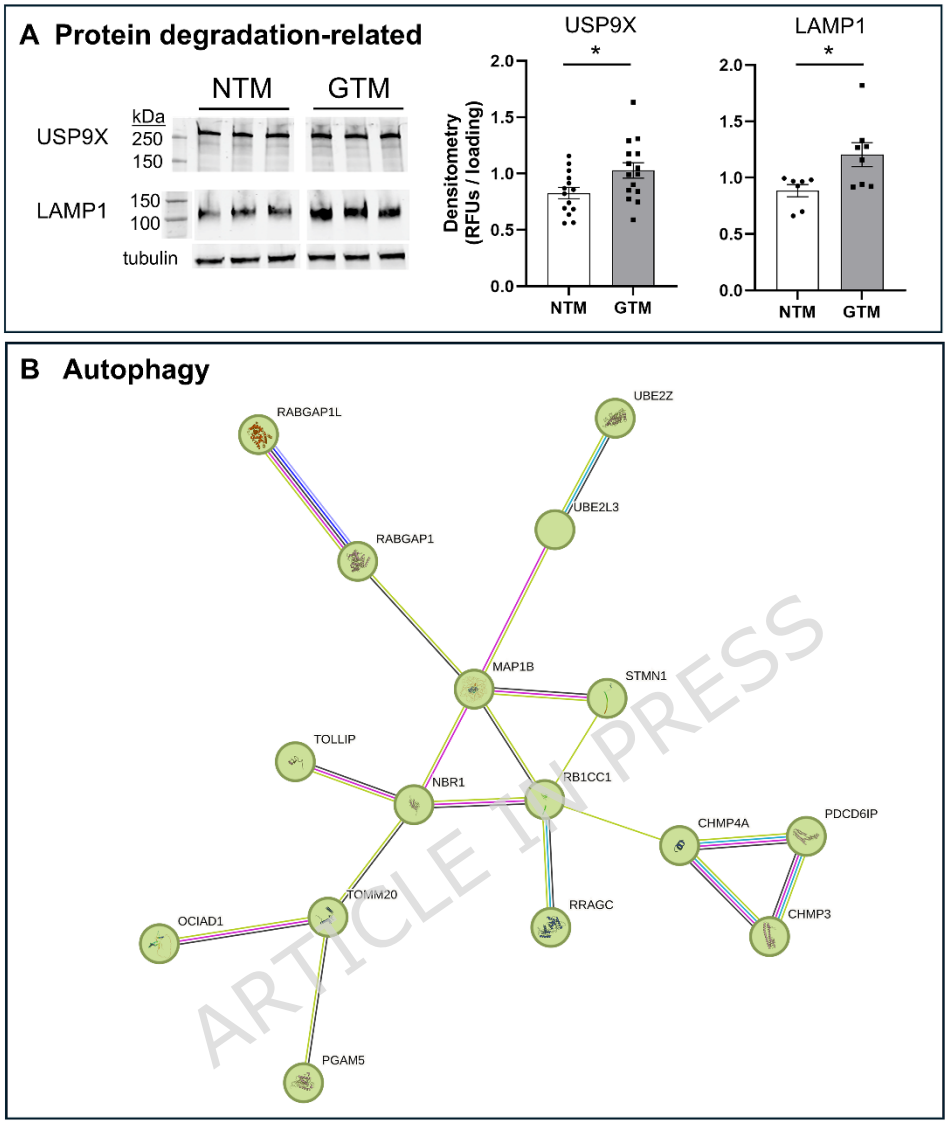


**Figure 5. Western immunoblot and densitometry of selected protein degradation pathway proteins.** (A) Ubiquitin Specific Peptidase 9 X-Linked (USP9X) and lysosomal-associated membrane protein 1 (LAMP1) are significantly upregulated in GTM cell lysates. Representative Western immunoblots show 3x NTM and 3x GTM cell strains, which are cropped from different parts of the same membranes. Original blots are presented in the Supplementary File. Densitometric quantitation is from n=15 biological replicates for USP9X and n=7 for LAMP1. Tubulin was used for loading control normalization. *$p<0.05$. (B) Sixteen proteins were associated with autophagy in GTM cells as depicted by STRING network analysis. Known interactions: cyan = from curated databases, pink = experimentally determined. Predicted interactions: green = gene neighborhood, blue=gene co-occurrence. Others: khaki = text mining, black = co-expression, lavender = protein homology. Filled nodes: a 3D structure is known or predicted.

We also investigated nuclear proteins. LMNA is an intermediate filament protein that is a component of the nuclear envelope, and it provides structural support for the nucleus[46]. In GTM cells, LMNA is upregulated 53-fold by TMTpro (Table 2) and Western immunoblotting showed LMNA is significantly upregulated in GTM cells (Figure 6A). DFFA is an endonuclease activated by caspase-3 that cleaves DNA during apoptosis[47]. DFFA was downregulated -1.4-fold in TMTpro analysis (Supplemental Table S4) and by Western immunoblotting (Figure 6A). Little is known about the function of SNX7, but it is strongly associated with the cell cycle, senescence, and DNA replication in hepatocellular carcinomas[48]. In GTM cells, SNX7 was upregulated 86-fold by TMTpro (Table 2). We performed immunofluorescence of NTM and GTM cells (Figure 6B). Both diseased and non-diseased cell strains showed small SNX7-labeled puncta throughout the cytosol, consistent with a role of SNX7 in endosomal trafficking and autophagy[49]. However, SNX7 also stained nucleoli, which has not been previously reported. This was confirmed by co-localizing with the nucleoli biomarker, nucleolin. We measured the number of nucleoli and their size using FIJI software. GTM cells were found to have fewer and significantly larger SNX7-labeled nucleoli than NTM cells ($p<0.05$; Figure 6B). Other nuclear proteins that were significantly changed were the upregulation of CHMP3 (1.6-fold), NEMP1 (1.5-fold) and HDAC1 (1.4-fold) in GTM cells, while RAD21 was downregulated (-1.3-fold). STRING interaction network analysis showed that 11 significantly regulated proteins were ribonuclear complex proteins (Figure 6C), while there were 12 proteins that localized to the nucleoli (Figure 6D).

**Figure 6**

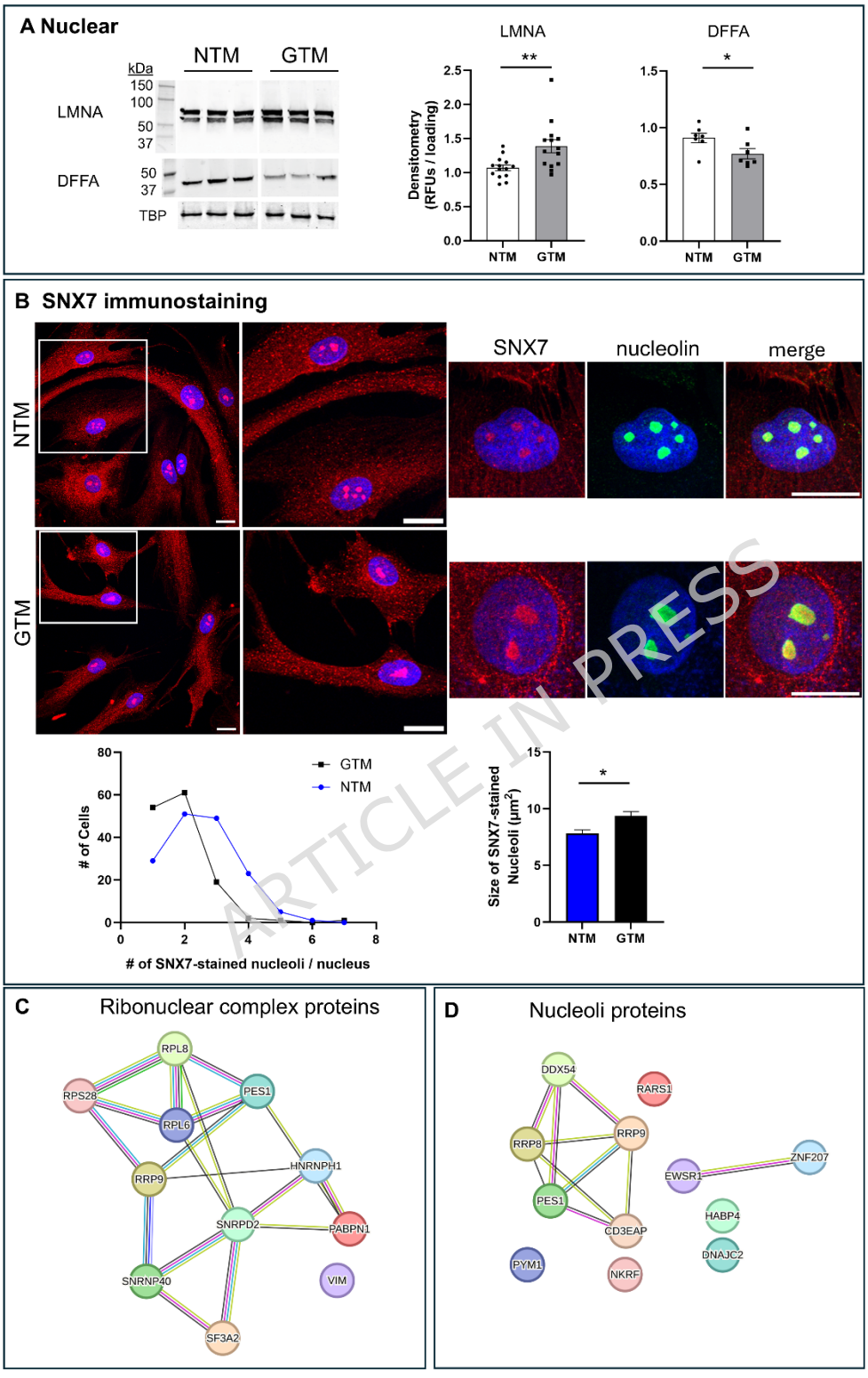


**Figure 6. Western immunoblot and densitometry of selected nuclear proteins.** (A) The nuclear protein lamin A/C (LMNA) is significantly upregulated in

GTM cells, while DNA fragmentation factor subunit alpha (DFFA) is significantly downregulated. Representative Western immunoblots show 3x NTM and 3x GTM cell strains, which are cropped from different parts of the same membranes. Original blots are presented in the Supplementary File. Densitometric quantitation is from n=14 biological replicates for LMNA or n=7 for DFFA. TATA-box-binding protein (TBP) was used as a loading control. *p<0.05; **p<0.01. (B) Sorting nexin 7 (SNX7) was localized to punctate endosomes in the cell cytosol as well as to the nucleoli in NTM and GTM cells. Boxed areas are shown at higher magnification to highlight the nucleoli staining. Colocalization of SNX7 and the nucleoli biomarker, nucleolin (green), in NTM and GTM cells is also shown. Scale bar = 20 µm. The number of SNX7-stained nucleoli were counted for NTM and GTM cells and there were fewer nucleoli per nucleus in GTM cells. FIJI software was used to measure the size of the nucleoli and GTM cells had significantly larger nucleoli. Data are from NTM cells (3 biological replicates, 160 cells) and GTM cells (2 biological replicates, 138 cells). * p=0.0019 by unpaired t-test. (C) In STRING interaction analysis, there were 11 proteins that were part of the ribonuclear protein complex. (D) Similarly, 12 proteins were identified as nucleoli proteins. Known interactions: cyan = from curated databases, pink = experimentally determined. Predicted interactions: green = gene neighborhood, blue=gene co-occurrence. Others: khaki = text mining, black = co-expression, lavender = protein homology.



Finally, we compared the 5518 TMTpro-labeled proteins identified in this study to genes identified by snRNAseq in non-glaucomatous human TM tissue[50]. In that paper, genes expressed in TM tissue were separated into three cell types termed ‘TM fibroblasts’, ‘uveal fibroblasts’, and ‘SC endothelial’. Since our TM cell cultures were derived from blunt dissected TM tissue containing all three of these cell types, we combined the three snRNAseq datasets to give a total of 4687 outflow pathway genes. When compared to the TMTpro-labeled proteins, there were 1752 molecules in common, with 3765 proteins not detected in the snRNAseq dataset and conversely, 2935 genes not detected in the proteomics dataset (Figure 7A). We also compared the significantly regulated TMT-labeled proteins (n=248) with glaucoma-associated genes (n=126) as well as genes associated with elevated IOP (n=124)[51,52]. Only 1 gene/protein was common to all 3 datasets: COL4A1 (Figure 7B).

Figure 7

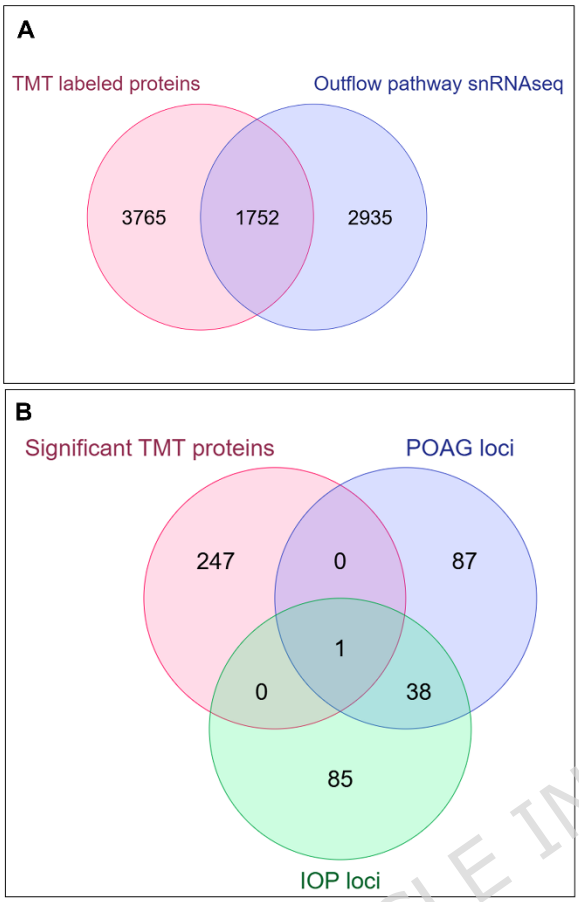




**Figure 7. Venn diagram showing TMT-labeled proteins and genes identified in RNAseq and GWAS studies.** (A) A Venn diagram showing TMT-labeled proteins identified in this study (n=5518) compared to TM outflow pathway genes identified by snRNAseq (n=4687). There were 1752 common genes/proteins between the two studies. Please note the snRNAseq dataset was from non-glaucomatous tissue only. (B) A Venn diagram showing TMTpro proteins that were differentially regulated in GTM cells (n=248) compared to glaucoma-associated genes (n=125) as well as genes associated with elevated IOP (n=123). Only one protein was common to all studies, which was COL4A1.

## Discussion

Glaucoma is a prevalent disease that affects millions of people worldwide, yet few proteomics studies have been performed on human ocular tissue[53]. This is largely due to the unavailability of donor eyes, small size of the tissue, and the significant loss of cells in POAG tissue[6]. Thus, protein concentrations per tissue are low, which hinders rigorous analysis. Recent studies have shown that primary GTM cells retain

molecular characteristics of the tissue from which they are derived and thus GTM cell cultures are useful *in vitro* model systems to study glaucoma[7,9,15]. In this study, we used GTM cells derived from human glaucomatous donor eyes and performed TMTpro isobaric-labeling quantitative proteomics to identify 248 significantly regulated proteins compared to age- and sex-matched non-glaucomatous TM cells. The TMTpro results reported in this study provide further support for dysfunction of Wnt signaling and protein degradation pathways, aberrant actin cytoskeletal regulation, and reveal alterations to nuclear proteins in glaucomatous TM cells.

Several studies have investigated protein differences between glaucoma and healthy TM. For instance, the extracellular protein cochlin was identified in glaucomatous TM tissue extracts, which were separated by SDS-PAGE and subject to LC-electrospray tandem mass spectrometry[19]. We did not detect cochlin by TMT proteomics in GTM cells, which may be due to our focus on analyzing the cell layer. However, PRR4 was upregulated both in our study and in theirs. Myocilin (MYOC) is the quintessential glaucoma-causing gene. MYOC mutations are present in approximately 5% of POAG patients[54] and prior studies have shown increased levels in the aqueous humor of POAG patients[55]. However, while MYOC was detected by TMTpro labeling in our study, there was no significant difference between NTM and GTM cells. This is likely because we selected TM cells that were wild type for MYOC missense mutations. Other proteins have previously been shown to be upregulated in glaucoma cells and tissues include secreted frizzled-related protein-1 (sFRP1) and clusterin[56,57], but these did not show significant differences between GTM and NTM in our study. However, we showed that CHI3L1 was significantly downregulated in GTM cells at both the gene and protein level[15], which is consistent with the TMTpro data presented here. Differences in the tissue extraction methods used in these prior studies, none of which included TMT labeling, likely explain the differences between the studies. Moreover, our study supplemented the culture media with ascorbate, which closely mimics the constituents of aqueous humor, and is an antioxidant and a cofactor for collagen synthesis.

Other groups have investigated the proteome of TM cells in response to IOP and or dexamethasone (DEX) treatment, a corticosteroid that can lead to secondary glaucoma. One study investigated the TM proteome in response to elevated IOP[34]. Human anterior segments were perfused *ex vivo* at either 1x or 2x pressure and

proteins were labeled with TMT reagents. While several ECM proteins were identified in common with the current study, it is difficult to directly compare the results of the two studies because they focused on non-diseased eyes, and the tissue was separated into regions of high and low aqueous outflow. For dexamethasone treatments, one study analyzed the cytoplasmic and membrane fractions of DEX-treated NTM cells and found 318 of 1644 proteins (12%) that were associated with the cytoskeleton[23]. Compared to our results, there were 19 cytoskeletal proteins in common between GTM and DEX-treated NTM cells. This included CFL1, CFL2, EPS8, MSN, ROCK2, and VIM. Another group analyzed the nuclear proteome of DEX-treated NTM cells by LC-MS/MS and found the levels of 48 proteins increased[58]. Their study and ours showed that EPS8, LIMCH1, and PYGB were upregulated. However, opposite effects were found for DCN. DCN was upregulated by DEX-treatment, but DCN was downregulated in GTM cells in our study. Previous studies showed that DCN had decreased immunostaining in POAG tissues[36]. Thus, decorin may serve opposite function in DEX-stimulated TM cells than in GTM cells. In a rat dexamethasone model of elevated IOP, TMT proteomics identified 292 differentially regulated proteins[35]. None overlapped with our study, likely because two different species were used. Together, these studies show that while there are some similarities between Dex-induced TM proteome and GTM cells, the POAG proteome is largely different.

Our enrichment analysis identified the cytoskeletal pathway as being significantly regulated in GTM cells. This is not surprising given the abundant literature that describes how actin stress fibers, cross-linked actin networks, and other alterations to the actin cytoskeleton are prevalent in glaucoma TM cells[38,59-61]. In fact, the actin cytoskeleton is the target of several anti-glaucoma medications. Of interest, the actin-binding proteins, ROCK2, TPM2, and MSN, were 3 of the 18 proteins that were detected in GTM cells, but not in NTM cells. Yet, all three proteins were detected in NTM cells in Western immunoblot and were upregulated in GTM cells, which was consistent with the TMTpro proteomics data. Increased ROCK2 in GTM cells is intriguing given that selective inhibition of the Rho/ROCK signaling pathway is the molecular basis of the newest class of FDA-approved glaucoma therapies[62]. ROCK2 activates LIM kinase, which in turn deactivates cofilin activity[43]. While both cofilin-1 and -2 were upregulated in GTM cells, we did not assess their activity. TPM2 has a role in stress fiber formation, and it is found to accumulate in the distal ends where

the stress fibers form focal adhesions, where it can control mechanosensitive contractility[63]. Upregulation of ROCK2, TPM2, and MSN in GTM cells presents additional cytoskeletal molecules that could aid design of novel glaucoma therapeutics. DIAPH2 immunostaining was in the perinuclear region but was more distended into the cytosol in GTM cells and surprisingly did not colocalize with the actin cytoskeleton. While DIAPH2 nucleates actin filaments,[64] it appears that it does not remain associated with the assembled SiR-labeled actin stress fibers in TM cells.

Protein degradation pathways were identified to be significantly regulated in GTM cells. Several of these proteins (e.g. SYVN1, UBE2L3, KCMF1) function to tag proteins with ubiquitin, targeting them for the proteasomal degradation pathway. Specifically, UBE2L3 catalyzes 'Lys-11'-linked polyubiquitination, which tags short-lived and abnormal proteins to the UPS pathway[65]. Its upregulation in GTM cells suggests that overall protein synthesis may be disrupted compared to old NTM cells. KCMF1 catalyzes ubiquitination and degradation of proteins that have been oxidized in response to reactive oxygen species[66], which plays a pathogenic role in the damage of glaucomatous TM cells. However, the deubiquitinase USP9X was also upregulated in GTM cells. USP9X has a very specific role in the TGFβ/BMP signaling pathway, where it removes ubiquitin from SMAD4. The TGFβ/SMAD pathway is activated in glaucoma TM[67], but the role of USP9X requires further investigation. The autophagy pathway was also identified as being significantly altered in GTM cells, with upregulation of LAMP1 and SNX7 among the proteins affected. Mitophagy, the selective autophagic removal of dysfunctional mitochondria, may also be affected because TOM20 and several mitochondrial NDUFS proteins are upregulated in GTM cells. Together, these data provide additional evidence for dysfunction in protein degradation pathways in GTM cells.

There were 18 proteins that were not detected above background counts in NTM cells. Of these, 44% were nuclear proteins. Studies suggest that there is a deterioration in the morphology and architecture of the nucleus during aging[68], disease[69], and during fibrosis[70]. LMNA, one of the 18 proteins not detected in NTM cells, is a component of the lamina underlying the inner nuclear envelope. Age-related defects in LMNA activation have been detected in fibroblasts[46]. Indeed, other studies have found that the nuclei of GTM cells have a larger volume, decreased chromatin condensation, and permissive histone acetylation compared to NTM cells[71]. Furthermore, nucleoli can

become enlarged/fragmented, which can drive ribosomal DNA instability[72]. Our SNX7 immunofluorescence results showed fewer, but significantly larger SNX7-stained nucleoli in GTM cells that age-matched NTM cells. This suggests that nucleoli number and size may be a biomarker of pathogenic TM cells[73]. SNX7 has not previously been localized to the nucleolus, but other autophagy biomarkers, such as LC3, can translocate to the nucleolus in TM cells in response to mechanical stress[74]. Thus, our proteomics data agrees with other studies that describe nuclear alterations in GTM cells. There is also increasing evidence that actin-associated proteins are associated with the nucleus[58]. Of the 18 proteins not detected in NTM cells, 33% were cytoskeletal proteins including ROCK2 and MSN. ROCK2 plays a central role in controlling actin assembly, but it is also localized to the nucleus where it interacts with phosphorylated STAT3[75]. MSN is primarily cytoplasmic, but along with other FERM domain-containing proteins, can localize in the nucleus [76]. It is not entirely clear why these proteins were not detected in TMT data of NTM cells, but they could be immunoblotted. However, it is possible that GTM-associated changes to the integrity of the nucleus may allow more efficient extraction of nuclear and cytoskeletal proteins from GTM cells by the cell scraping and bead-beating methods employed in this study.

There are several limitations of this study. First, there were only five NTM and GTM cell strains each used in the TMTpro analysis. However, additional biological cell strains were evaluated by Western immunoblotting, which validated the TMTpro data. Second, we had limited clinical information on the glaucoma patients. Differences between disease severity, the medications they were prescribed, and how long they had been taking them may significantly affect protein synthesis and degradation. Third, all our cell strains were derived from Caucasian individuals so the results may not extrapolate to other populations. Fourth, while certain proteins showed similarity in their levels between cultured cells and tissues e.g. DCN is decreased in glaucoma, there remains a possibility that the changes detected in cells do not fully replicate those in tissues. Finally, quantitative bottom-up proteomics methods share some limitations. Ratio distortion is unlikely to be an issue because we used MS3 scans to generate reporter ion signals, which increases accuracy,[31] but there is still a discrepancy between the magnitude of fold changes detected by TMTpro and Western blotting. For instance, MSN showed a 15-fold increase in TMTpro, but a

modest 1.5-fold increase by Western immunoblotting. Western immunoblotting depends on a multitude of factors: solubilization of the protein from cell lysates, transfer of proteins to the Western membrane, primary antibody specificity, and detection of the primary with a secondary antibody. At any point, there can be loss of signal and it has even been argued that Western immunoblotting is not a good method to validate MS data.[77] However, while the magnitude of the fold changes is different for several proteins in our study, in each case, both methods show the same trend i.e. up- or downregulation. When proteins are digested for MS analysis, there is potential loss of information about different proteoforms. Quantitative summarization relies on many assumptions made by protein inference logic. The use of canonical reference proteomes (one protein per gene FASTA files) and parsimonious protein grouping are conservative approaches to bottom-up protein quantitation. Thus, it was not possible to explore protein isoforms, protein amino acid substitutions, and post-translational modifications with the experimental approach utilized in this study.

In summary, our quantitative proteomics study identified 248 significantly regulated proteins in cultured GTM cells. We validated a subset of these proteins by Western immunoblotting and immunofluorescence, although the function of other differentially abundant proteins remains to be investigated. Our results confirm several proteins and pathways that are known to be involved in glaucoma pathogenesis but also identify new protein targets that could aid in the development of clinical therapies for glaucoma patients.



## Methods

### *Experimental Design and Statistical Rationale*

All cell strains were genotyped for myocilin exon 3, where 93% of the myocilin glaucoma-causing mutations reside[78]. NTM (n=9) and GTM (n=9) were labeled with TMTpro reagents, and a subset were chosen for analysis (Table 1). For Western immunoblot and immunofluorescence assays, we used cell strains that were disease-matched and genotyped as above (‘n’ is noted in each figure legend). Statistical tests used for each assay are described within each section below.

### *Materials*

Cell culture reagents including Dulbecco's Modified Eagles Medium (DMEM), antibiotic-antimycotic, sterile phosphate-buffered saline (PBS), proteomics reagents including triethylammonium bicarbonate (TEAB), TMTpro isobaric reagents, an Acclaim PepMap 100 µm × 2 cm NanoViper C18, 5 µm trap, the PepMap RSLC C18, 2 µm, 75 µm × 25 cm EasySpray column, organic solvents, and the Pierce peptide and BCA protein assay kits, and immunofluorescence supplies including CAS-block histochemical reagent, Alexa-fluor-conjugated secondary antibodies, and DAPI-containing ProlongGold, were from Thermo Fisher Scientific (Waltham, MA). A NanoEase 5 µm XBridge BEH130 C18 300 µm × 50 mm column was from Waters Corporation (Milford, MA), while S-Traps were from Protifi, Inc (Fairport, NY). Fetal bovine serum, acid-washed glass beads (PN#G8772-10G), ascorbate, and other chemicals were from MilliporeSigma (St. Louis, MO). BlastR lysis buffer and BlastR filters were from Cytoskeleton, Inc. (Denver, CO). Pre-cast SDS-PAGE gels were from Bio-Rad Laboratories (Hercules, CA). Collagen I-coated BioFlex cell culture plates were from FlexCell International Corp (Burlington, NC). All primary antibodies and their commercial sources are listed in Supplementary Table S1. Licor blocking buffer was from LicorBio (Lincoln, NE) and IRDye secondary antibodies for Western immunoblots were from Rockland Immunochemicals (Gilbert, PA).

### *Culture of Trabecular Meshwork Cells*

Primary TM cells were grown following the published guidelines for culturing and characterizing TM cells[8]. Studies using human cadaver TM tissue are "not research involving human subjects" as determined by the OHSU Institutional Review Board (STUDY00025374) and there were no living human participants in the study. All studies followed the principles outlined in the Declaration of Helsinki for use of human tissue for medical research. Demographics of the donors are shown in Table 1. All cell strains were characterized by their ability to upregulate myocilin expression in response to dexamethasone treatment, which is either shown here (Supplemental Figure S1), or has been published previously[15,16,79]. For proteomics experiments, TM cells were used at passage number 3, while for Western immunoblot and immunofluorescence analysis, cells were used at passages 4 and 5.

TM cells were grown to confluence in 6-well plates in DMEM supplemented with 10% fetal bovine serum and 1% antibiotic-antimycotic. After 3 days in culture, the media

was exchanged to serum-free DMEM supplemented with 0.1 mM ascorbate. Cells were cultured for an additional 3 days. After washing in PBS, cells were scraped into 1 ml of PBS and centrifuged at 2000xg to pellet cells and associated ECM proteins. The supernatant was removed, and pellets were frozen at -80 $^{o}$C.

***Sample Preparation and Trypsin Digestion***

Samples were prepared by adding 200 µl of 5% sodium dodecyl sulfate (SDS) and 40-50 mg of acid-washed glass beads, which were previously rinsed in $dH_2O$. Cell extracts were then homogenized by bead-beating at 4 $^{o}$C in a Bertin Precellys Evolution Bead Beater (6 cycles of 15 sec at 6800 rpm with a 30 sec pause between cycles) as described previously[34]. Samples were then heated to 70 $^{o}$C for 10 min, centrifuged for 5 min at 8000xg, and sonicated in a Diagenode Bioruptor Pico with the following conditions (30 sec on, 30 sec off, 10 cycles). After centrifugation at 12,000xg for 10 min, the protein concentration in each sample was measured by BCA assay.

SDS protein extraction buffer (5% SDS, 50 mM TEAB (pH7.5) and 22 mM DTT was then added to each sample and incubated for 10 min at 95 °C. Samples were alkylated by adding 40 mM IAA (final concentration) and incubated at room temp in the dark for 30 min. Phosphoric acid (1.2% final concentration) and 6x volume of S-Trap protein binding buffer (90% aqueous methanol containing 100 mM TEAB, pH7.5) was then added to each sample. The acidified SDS lysate/MeOH S-Trap buffer mixture was then loaded into the S-Trap micro column, which was centrifuged for 3 min at 4,000xg until all the sample had passed through. Captured protein was washed 5 times with S-Trap protein binding buffer and then 40 µl of digestion buffer (80 ng/µL trypsin in 50 mM TEAB at a 1:16 enzyme: substrate ratio) was loaded into the top of the micro column, which was loosely capped and incubated overnight at 37 $^{o}$C. The next day, 40 µL each of 50mM TEAB, 0.2% aqueous formic acid, and 50%/50% 0.2% formic acid/acetonitrile were added, the columns were shaken for 10 min, and the column spun at 12,000xg for 5 min to elute the digested peptides. Concentration was determined with a Pierce peptide assay kit and samples were dried by vacuum centrifugation.

***TMTpro labeling***

A tandem mass tag (TMTpro) 18-plex reagent kit was used to label the digested peptide samples. Each TMTpro 18-plex reagent (200 µg), dissolved in 12 µl of anhydrous acetonitrile (ACN), was added to 15 µg of peptide sample in 20 µl of 100mM TEAB, and labeling performed by shaking at room temp for 1h. After incubation, 2 µl of the labeled peptide digest from each sample were combined into one tube, then 2 µl of 5% hydroxylamine was added, samples incubated at room temp for 15 min and dried by vacuum centrifugation. The remaining volume of each labeled sample was frozen at −80 °C without hydroxylamine addition (in case relabeling was required). The combined TMTpro labeled sample was then dissolved in 20 µl of 5% formic acid and 2 µg of peptides analyzed using a 140 min LC-MS/MS method on an Orbitrap Fusion Mass Spectrometer to check labeling efficiency and determine the volume of each sample to provide equal total reporter ion intensities in the combined sample for the 2D-LC/MS analysis. The TMTpro labeled samples were thawed and calculated aliquots removed that would produce 50 µg of total peptides from all 18 samples. To quench the labeling reaction, 5% hydroxylamine was added to bring the total hydroxylamine concentration to 0.5% followed by incubation for 15 min at room temperature.

***Two-dimensional liquid chromatography/mass spectrometry (LC-MS)***

The multiplexed samples were dissolved in 10 mM ammonium formate, pH 9 buffer and injected onto a NanoEase 5 µm XBridge BEH130 C18 300 µm × 50 mm column at 3 µl/min in a mobile phase containing 10 mM ammonium formate (pH 9). Peptides were eluted by sequential injection of 20 µl volumes of 17, 20, 21, 22, 23, 24, 25, 26, 27, 28, 29, 30, 31, 32, 33, 34, 35, 40, 50, and 90% ACN (20 fractions). Eluted peptides were diluted at a 3-way union with mobile phase containing 0.1% formic acid at a 24 µl/min flow rate and delivered to an Acclaim PepMap 100 µm × 2 cm NanoViper C18, 5 µm trap on a switching valve. After 10 min of loading, the trap column was switched on-line to a PepMap RSLC C18, 2 µm, 75 µm × 25 cm EasySpray column. TMTpro-labeled peptides were then separated at low pH in the second dimension using a 5–25% ACN gradient over 100 min in the mobile phase containing 0.1% formic acid at a 300 nL/min flow rate.

Tandem mass spectrometry data was collected using an Orbitrap Fusion Tribrid instrument configured with an EasySpray NanoSource (Thermo Fisher Scientific).

Survey scans were performed in the Orbitrap mass analyzer at resolution = 120,000, with internal mass calibration enabled, and data-dependent MS2 scans using dynamic exclusion performed in the linear ion trap using collision-induced dissociation. Reporter ion detection was performed in the Orbitrap mass analyzer (resolution = 50,000) with higher-energy collisional dissociation in the ion-routing multipole using MS3 scans after synchronous precursor isolation of the top 10 fragment ions in the linear ion trap. There were 369,982 MS2/MS3 instrument scans acquired from the 20-fractions.

***TMTpro data analysis***

The 20 binary instrument files were processed with the PAW pipeline[80]. Binary files were converted to text files using MSConvert[81]. Python scripts extracted TMT reporter ion peak heights and fragment ion spectra in MS2 format. The Comet search engine (version 2016.03) was used[82]: 1.25 Da monoisotopic peptide mass tolerance, 1.0005 Da monoisotopic fragment ion tolerance, tryptic cleavage with up to three missed cleavages, variable oxidation of methionine residues (+15.9949 Da), static alkylation of cysteines (+57.0215 Da), and static modifications for TMTpro labels (+304.2071 Da at peptide N-termini and at lysine residues). Searches used UniProt proteome UP000005640 (Homo sapiens, taxon ID 9606) canonical FASTA sequences (20,593 proteins, downloaded June 2023). Common contaminants (175 sequences excluding any albumins) were added, and sequence-reversed entries were concatenated for a final protein FASTA file of 41,536 sequences.

Top-scoring peptide spectrum matches (PSMs) were filtered to a 1% false discovery rate (FDR) using interactive delta-mass and conditional peptide-prophet-like linear discriminant function scores[83]. Incorrect delta-mass and score histogram distributions were estimated using the target/decoy method. The filtered PSMs (129,424 scans) were assembled into protein lists using basic and extended parsimony principles and required two distinct peptides per protein. The final list of identified proteins, protein groups, and protein families (5,518 total) were used to define unique and shared peptides for quantitative use. Total (summed) reporter ion intensities were computed from the PSMs associated with all unique peptides for each protein.

The protein intensity values for each biological sample in each biological condition were compared for differential protein abundance using the Bioconductor package

edgeR[84] and the Trimmed Mean of M-values (TMM) biological normalization function[85]. Benjamini-Hochberg corrected p-values (FDR < 0.1) were considered as candidates for differential relative abundance for TMTpro data. Pathway analysis of 248 significantly differentially abundant proteins was performed using ShinyGO (v0.85; https://bioinformatics.sdstate.edu/go/)[86] and STRING (https://string-db.org/)[87]. Gene enrichment pathways were plotted using SRplot (https://www.bioinformatics.com.cn/en). Raw data is in Supplemental Table S1.

***Western Immunoblotting***

NTM and GTM cells were grown in T25 flasks for 3 days in DMEM + 10% FCS and then exchanged to serum-free DMEM supplemented with 0.1 mM ascorbate for an additional 3 days. Conditioned media was collected. The TM cell layers were extracted with BlastR lysis buffer and genomic DNA was removed using BlastR filters following the manufacturer's directions. Proteins were reduced (10mM dithiothreitol) and separated on either precast 10% or 4-15% SDS-PAGE gels depending on their molecular weights. Some gels were stained with Coomassie blue to evaluate protein loading. Proteins were transferred to nitrocellulose membranes (0.45 µm) and blocked with Licor blocking buffer. Membranes were probed with one or more of the primary antibodies (Supplemental Table S2) and, after washing in PBS + 0.1% Tween-20, IRDye800 or IRDye700-conjugated secondary antibodies were incubated. Western immunoblots and Coomassie stained gels were imaged on an Odyssey DLx imager (LicorBio). Uncropped images of all Western blots can be found in the supplemental data. Band intensities were quantitated with FIJI software (https://imagej.net/software/fiji/). After background pixels were subtracted, the relative fluorescent unit (RFU) of each band was then normalized to either tubulin (cell lysates), TATA-box binding protein (TBP; nucleus), or to the entire vertical lane of a Coomassie-stained gel (conditioned media). Data points were plotted on a scatter plot with a bar showing the standard error of the mean (S.E.M.) and analyzed using an unpaired t-test (GraphPad Prism, Boston, MA), where $p<0.05$ was considered statistically significant.

***Immunofluorescence***

Primary NTM and GTM cells were plated in collagen I-coated BioFlex plates with DMEM + 10% FCS, as described previously[15,16] and incubated for 24 hours. Some cells were

labeled with 0.1 µM SiR-actin and 10 µM verapamil (Cytoskeleton, Inc, Denver, CO) to label the actin cytoskeleton, which was added for the final hour of culture. Cells were either fixed with 4% paraformaldehyde (for SiR-stained cells) for 5 mins, or with ice-cold methanol for 3 mins. Fixed cells were blocked with CAS-block histochemical reagent, and incubated with DIAPH2, SNX7, or nucleolin primary antibodies (Supplemental Table S2). Cells were washed and incubated with Alexa-fluor 488-conjugated donkey anti-mouse and Alexa-fluor 594-conjugated donkey anti-rabbit secondary antibodies for 30 min. After washing, coverslips were mounted in DAPI-containing ProlongGold and images were acquired with a Fluoview FV1000 confocal microscope (Olympus, Waltham, MA). FIJI software was used to process raw files. To measure size of nucleoli, the SNX7 channel was processed by adjusting the threshold, converting it into a binary image, and then using the 'analyze particles' function, where the size was set to '2 µm – infinity'. Data were averaged from NTM cells (3 biological replicates, 160 cells) and GTM cells (2 biological replicates, 138 cells). Data points were plotted on a frequency plot and a bar chart, and an unpaired t-test was used to determine significance (GraphPad Prism).



**Acknowledgements**

We thank VisionGift, Portland, OR for helping to procure human donor eyes.

**Funding declaration**

Supported by NIH/NEI grants R01 EY032590 (KEK), R01 EY019643 (KEK), the Malcolm M. Marquis MD endowed fund for innovation, and an unrestricted grant from Research to Prevent Blindness (New York, NY) to the Casey Eye Institute, OHSU. Mass spectrometric analysis was performed by the OHSU Proteomics Shared Resource (RRID: SCR_009991) with partial support from NIH core grants P30EY010572, P30CA069533, and S10OD012246.

**Author contributions**

PH, APR, KEK conceived and designed the study; PH, YYS, KZ conducted experiments; PAW, APR, KEK, PH analyzed data. KEK, PAW, PH wrote the manuscript. All authors reviewed the manuscript.

### *Data Availability*

Data sets generated from the mass spectrometry proteomics analysis have been deposited to the ProteomeXchange Consortium (http://proteomecentral.proteomexchange.org) via the PRIDE partner repository with the data set identifier PXD066598.[88]

**Competing interests:** The authors declare no competing interests.

**Supplemental data**

This article contains supplemental data.


1 Jayaram, H., Kolko, M., Friedman, D. S. & Gazzard, G. Glaucoma: now and beyond. *Lancet* **402**, 1788-1801, (2023).

2 Acott, T. S., Vranka, J. A., Keller, K. E., Raghunathan, V. & Kelley, M. J. Normal and glaucomatous outflow regulation. *Prog Retin Eye Res* **82**, 100897, (2021).

3 Tamm, E. R., Braunger, B. M. & Fuchshofer, R. Intraocular Pressure and the Mechanisms Involved in Resistance of the Aqueous Humor Flow in the Trabecular Meshwork Outflow Pathways. *Prog Mol Biol Transl Sci* **134**, 301-314, (2015).

4 Keller, K. E. & Peters, D. M. Pathogenesis of glaucoma: Extracellular matrix dysfunction in the trabecular meshwork-A review. *Clin Exp Ophthalmol*, (2022).

5 Tian, B., Gabelt, B. T., Geiger, B. & Kaufman, P. L. The role of the actomyosin system in regulating trabecular fluid outflow. *Exp Eye Res* **88**, 713-717, (2009).

6 Alvarado, J., Murphy, C. & Juster, R. Trabecular meshwork cellularity in primary open-angle glaucoma and nonglaucomatous normals. *Ophthalmology* **91**, 564-579, (1984).

7 Stamer, D. W., Roberts, B. C., Epstein, D. L. & Allingham, R. R. Isolation of primary open-angle glaucomatous trabecular meshwork cells from whole eye tissue. *Curr Eye Res* **20**, 347-350, (2000).

8 Keller, K. E. *et al.* Consensus recommendations for trabecular meshwork cell isolation, characterization and culture. *Exp Eye Res* **171**, 164-173, (2018).

9 Stamer, W. D. & Clark, A. F. The many faces of the trabecular meshwork cell. *Exp Eye Res* **158**, 112-123, (2017).

10 Tovar-Vidales, T., Roque, R., Clark, A. F. & Wordinger, R. J. Tissue transglutaminase expression and activity in normal and glaucomatous human trabecular meshwork cells and tissues. *Invest Ophthalmol Vis Sci* **49**, 622-628, (2008).

11 Balestrini, J. L., Chaudhry, S., Sarrazy, V., Koehler, A. & Hinz, B. The mechanical memory of lung myofibroblasts. *Integr Biol (Camb)* **4**, 410-421, (2012).

12 Cambria, E. *et al.* Linking cell mechanical memory and cancer metastasis. *Nat Rev Cancer* **24**, 216-228, (2024).
13 Tamm, E. R., Siegner, A., Baur, A. & Lutjen-Drecoll, E. Transforming growth factor-beta 1 induces alpha-smooth muscle-actin expression in cultured human and monkey trabecular meshwork. *Exp Eye Res* **62**, 389-397, (1996).
14 de Kater, A. W., Shahsafaei, A. & Epstein, D. L. Localization of smooth muscle and nonmuscle actin isoforms in the human aqueous outflow pathway. *Invest Ophthalmol Vis Sci* **33**, 424-429, (1992).
15 Yang, Y. F. *et al.* Fibrosis-Related Gene and Protein Expression in Normal and Glaucomatous Trabecular Meshwork Cells. *Invest Ophthalmol Vis Sci* **66**, 48, (2025).
16 Sun, Y. Y., Bradley, J. M. & Keller, K. E. Phenotypic and Functional Alterations in Tunneling Nanotubes Formed by Glaucomatous Trabecular Meshwork Cells. *Invest Ophthalmol Vis Sci* **60**, 4583-4595, (2019).
17 Peters, J. C., Bhattacharya, S., Clark, A. F. & Zode, G. S. Increased Endoplasmic Reticulum Stress in Human Glaucomatous Trabecular Meshwork Cells and Tissues. *Invest Ophthalmol Vis Sci* **56**, 3860-3868, (2015).
18 Porter, K., Hirt, J., Stamer, W. D. & Liton, P. B. Autophagic dysregulation in glaucomatous trabecular meshwork cells. *Biochim Biophys Acta* **1852**, 379-385, (2015).
19 Bhattacharya, S. K. *et al.* Proteomics reveal Cochlin deposits associated with glaucomatous trabecular meshwork. *J Biol Chem* **280**, 6080-6084, (2005).
20 Elsobky, S., Crane, A. M., Margolis, M., Carreon, T. A. & Bhattacharya, S. K. Review of application of mass spectrometry for analyses of anterior eye proteome. *World J Biol Chem* **5**, 106-114, (2014).
21 Bollinger, K. E. *et al.* Quantitative proteomics: TGFbeta(2) signaling in trabecular meshwork cells. *Invest Ophthalmol Vis Sci* **52**, 8287-8294, (2011).
22 Steely, H. T. *et al.* Protein expression in a transformed trabecular meshwork cell line: proteome analysis. *Mol Vis* **12**, 372-383, (2006).
23 Clark, R. *et al.* Comparative genomic and proteomic analysis of cytoskeletal changes in dexamethasone-treated trabecular meshwork cells. *Mol Cell Proteomics* **12**, 194-206, (2013).
24 Soundararajan, A. *et al.* Multiomics analysis reveals the mechanical stress-dependent changes in trabecular meshwork cytoskeletal-extracellular matrix interactions. *Front Cell Dev Biol* **10**, 874828, (2022).
25 Chowdhury, U. R., Madden, B. J., Charlesworth, M. C. & Fautsch, M. P. Proteome analysis of human aqueous humor. *Invest Ophthalmol Vis Sci* **51**, 4921-4931, (2010).
26 Hubens, W. H. G. *et al.* Aqueous humor proteome of primary open angle glaucoma: A combined dataset of mass spectrometry studies. *Data Brief* **32**, 106327, (2020).
27 Liu, X. *et al.* Proteome Characterization of Glaucoma Aqueous Humor. *Mol Cell Proteomics* **20**, 100117, (2021).
28 McDonnell, F. S., Riddick, B. J., Roberts, H., Skiba, N. & Stamer, W. D. Comparison of the extracellular vesicle proteome between glaucoma and non-glaucoma trabecular meshwork cells. *Front Ophthalmol (Lausanne)* **3**, (2023).
29 Stamer, W. D., Hoffman, E. A., Luther, J. M., Hachey, D. L. & Schey, K. L. Protein profile of exosomes from trabecular meshwork cells. *Journal of proteomics* **74**, 796-804, (2011).

30 Micera, A. *et al.* Differential Protein Expression Profiles in Glaucomatous Trabecular Meshwork: An Evaluation Study on a Small Primary Open Angle Glaucoma Population. *Adv Ther* **33**, 252-267, (2016).
31 McAlister, G. C. *et al.* MultiNotch MS3 enables accurate, sensitive, and multiplexed detection of differential expression across cancer cell line proteomes. *Anal Chem* **86**, 7150-7158, (2014).
32 Li, J. *et al.* TMTpro-18plex: The Expanded and Complete Set of TMTpro Reagents for Sample Multiplexing. *J Proteome Res* **20**, 2964-2972, (2021).
33 Thompson, A. *et al.* Tandem mass tags: a novel quantification strategy for comparative analysis of complex protein mixtures by MS/MS. *Anal Chem* **75**, 1895-1904, (2003).
34 Vranka, J. A. *et al.* Biomechanical Rigidity and Quantitative Proteomics Analysis of Segmental Regions of the Trabecular Meshwork at Physiologic and Elevated Pressures. *Invest Ophthalmol Vis Sci* **59**, 246-259, (2018).
35 Liang, X., Li, N., Rong, Y., Wang, J. & Zhang, H. Identification of proteomic changes for dexamethasone-induced ocular hypertension using a tandem mass tag (TMT) approach. *Exp Eye Res* **216**, 108914, (2022).
36 Schneider, M. *et al.* A novel ocular function for decorin in the aqueous humor outflow. *Matrix Biol* **97**, 1-19, (2021).
37 Colorado, P. C. *et al.* Anti-angiogenic cues from vascular basement membrane collagen. *Cancer Res* **60**, 2520-2526, (2000).
38 Rao, P. V., Pattabiraman, P. P. & Kopczynski, C. Role of the Rho GTPase/Rho kinase signaling pathway in pathogenesis and treatment of glaucoma: Bench to bedside research. *Exp Eye Res* **158**, 23-32, (2017).
39 Iontcheva, I., Amar, S., Zawawi, K. H., Kantarci, A. & Van Dyke, T. E. Role for moesin in lipopolysaccharide-stimulated signal transduction. *Infect Immun* **72**, 2312-2320, (2004).
40 Stamenkovic, I. & Yu, Q. Merlin, a "magic" linker between extracellular cues and intracellular signaling pathways that regulate cell motility, proliferation, and survival. *Curr Protein Pept Sci* **11**, 471-484, (2010).
41 Lin, J. J., Eppinga, R. D., Warren, K. S. & McCrae, K. R. Human tropomyosin isoforms in the regulation of cytoskeleton functions. *Adv Exp Med Biol* **644**, 201-222, (2008).
42 Yeoh, S., Pope, B., Mannherz, H. G. & Weeds, A. Determining the differences in actin binding by human ADF and cofilin. *J Mol Biol* **315**, 911-925, (2002).
43 Rao, V. P. & Epstein, D. L. Rho GTPase/Rho kinase inhibition as a novel target for the treatment of glaucoma. *BioDrugs* **21**, 167-177, (2007).
44 Keller, K. E. *et al.* Ankyrin repeat and suppressor of cytokine signaling box containing protein-10 is associated with ubiquitin-mediated degradation pathways in trabecular meshwork cells. *Mol Vis* **19**, 1639-1655, (2013).
45 Liton, P. B. The autophagic lysosomal system in outflow pathway physiology and pathophysiology. *Exp Eye Res* **144**, 29-37, (2016).
46 Scaffidi, P. & Misteli, T. Lamin A-dependent nuclear defects in human aging. *Science* **312**, 1059-1063, (2006).
47 Liu, X., Zou, H., Slaughter, C. & Wang, X. DFF, a heterodimeric protein that functions downstream of caspase-3 to trigger DNA fragmentation during apoptosis. *Cell* **89**, 175-184, (1997).
48 Chen, J., Gao, G., Zhang, Y., Dai, P. & Huang, Y. Comprehensive analysis and validation of SNX7 as a novel biomarker for the diagnosis, prognosis, and

prediction of chemotherapy and immunotherapy response in hepatocellular carcinoma. *BMC Cancer* **23**, 899, (2023).

49 Anton, Z. *et al.* A heterodimeric SNX4--SNX7 SNX-BAR autophagy complex coordinates ATG9A trafficking for efficient autophagosome assembly. *J Cell Sci* **133**, (2020).

50 van Zyl, T. *et al.* Cell atlas of the human ocular anterior segment: Tissue-specific and shared cell types. *Proc Natl Acad Sci U S A* **119**, e2200914119, (2022).

51 Gharahkhani, P. *et al.* Genome-wide meta-analysis identifies 127 open-angle glaucoma loci with consistent effect across ancestries. *Nat Commun* **12**, 1258, (2021).

52 Khawaja, A. P. *et al.* Genome-wide analyses identify 68 new loci associated with intraocular pressure and improve risk prediction for primary open-angle glaucoma. *Nat Genet* **50**, 778-782, (2018).

53 Ahmad, M. T., Zhang, P., Dufresne, C., Ferrucci, L. & Semba, R. D. The Human Eye Proteome Project: Updates on an Emerging Proteome. *Proteomics* **18**, e1700394, (2018).

54 Saccuzzo, E. G., Youngblood, H. A. & Lieberman, R. L. Myocilin misfolding and glaucoma: A 20-year update. *Prog Retin Eye Res* **95**, 101188, (2023).

55 Howell, K. G., Vrabel, A. M., Chowdhury, U. R., Stamer, W. D. & Fautsch, M. P. Myocilin levels in primary open-angle glaucoma and pseudoexfoliation glaucoma human aqueous humor. *J Glaucoma* **19**, 569-575, (2010).

56 Wang, W. H. *et al.* Increased expression of the WNT antagonist sFRP-1 in glaucoma elevates intraocular pressure. *J Clin Invest* **118**, 1056-1064, (2008).

57 Soundararajan, A., Wang, T., Ghag, S. A., Kang, M. H. & Pattabiraman, P. P. Novel insight into the role of clusterin on intraocular pressure regulation by modifying actin polymerization and extracellular matrix remodeling in the trabecular meshwork. *J Cell Physiol* **237**, 3012-3029, (2022).

58 Bachman, W. *et al.* Glucocorticoids Preferentially Influence Expression of Nucleoskeletal Actin Network and Cell Adhesive Proteins in Human Trabecular Meshwork Cells. *Front Cell Dev Biol* **10**, 886754, (2022).

59 Bermudez, J. Y., Montecchi-Palmer, M., Mao, W. & Clark, A. F. Cross-linked actin networks (CLANs) in glaucoma. *Exp Eye Res* **159**, 16-22, (2017).

60 Keller, K. E. & Kopczynski, C. Effects of Netarsudil on Actin-Driven Cellular Functions in Normal and Glaucomatous Trabecular Meshwork Cells: A Live Imaging Study. *J Clin Med* **9**, (2020).

61 Filla, M. S., Schwinn, M. K., Sheibani, N., Kaufman, P. L. & Peters, D. M. Regulation of cross-linked actin network (CLAN) formation in human trabecular meshwork (HTM) cells by convergence of distinct beta1 and beta3 integrin pathways. *Invest Ophthalmol Vis Sci* **50**, 5723-5731, (2009).

62 Wang, S. K. & Chang, R. T. An emerging treatment option for glaucoma: Rho kinase inhibitors. *Clin Ophthalmol* **8**, 883-890, (2014).

63 Gateva, G. *et al.* Tropomyosin Isoforms Specify Functionally Distinct Actin Filament Populations In Vitro. *Curr Biol* **27**, 705-713, (2017).

64 Wallar, B. J. & Alberts, A. S. The formins: active scaffolds that remodel the cytoskeleton. *Trends Cell Biol* **13**, 435-446, (2003).

65 Zhang, X. *et al.* Mechanism and Disease Association With a Ubiquitin Conjugating E2 Enzyme: UBE2L3. *Front Immunol* **13**, 793610, (2022).

66 Heo, A. J. *et al.* The N-terminal cysteine is a dual sensor of oxygen and oxidative stress. *Proc Natl Acad Sci U S A* **118**, (2021).

67 McDowell, C. M., Tebow, H. E., Wordinger, R. J. & Clark, A. F. Smad3 is necessary for transforming growth factor-beta2 induced ocular hypertension in mice. *Exp Eye Res* **116**, 419-423, (2013).

68 Pathak, R. U., Soujanya, M. & Mishra, R. K. Deterioration of nuclear morphology and architecture: A hallmark of senescence and aging. *Ageing Res Rev* **67**, 101264, (2021).

69 Gauthier, B. R. & Comaills, V. Nuclear Envelope Integrity in Health and Disease: Consequences on Genome Instability and Inflammation. *Int J Mol Sci* **22**, (2021).

70 McDonald, O. G., Wu, H., Timp, W., Doi, A. & Feinberg, A. P. Genome-scale epigenetic reprogramming during epithelial-to-mesenchymal transition. *Nat Struct Mol Biol* **18**, 867-874, (2011).

71 Ghosh, R. *et al.* Altered nuclear dynamics in glaucomatous trabecular meshwork cell pathobiology. *Invest Ophthalmol & Visual Sci* **66**, 3253, (2025).

72 Gutierrez, J. I. & Tyler, J. K. A mortality timer based on nucleolar size triggers nucleolar integrity loss and catastrophic genomic instability. *Nat Aging* **4**, 1782-1793, (2024).

73 Liton, P. B. *et al.* Cellular senescence in the glaucomatous outflow pathway. *Exp Gerontol* **40**, 745-748, (2005).

74 Shim, M. S., Nettesheim, A., Hirt, J. & Liton, P. B. The autophagic protein LC3 translocates to the nucleus and localizes in the nucleolus associated to NUFIP1 in response to cyclic mechanical stress. *Autophagy* **16**, 1248-1261, (2020).

75 Chen, W. *et al.* ROCK2, but not ROCK1 interacts with phosphorylated STAT3 and co-occupies TH17/TFH gene promoters in TH17-activated human T cells. *Sci Rep* **8**, 16636, (2018).

76 Batchelor, C. L., Woodward, A. M. & Crouch, D. H. Nuclear ERM (ezrin, radixin, moesin) proteins: regulation by cell density and nuclear import. *Exp Cell Res* **296**, 208-222, (2004).

77 Aebersold, R., Burlingame, A. L. & Bradshaw, R. A. Western blots versus selected reaction monitoring assays: time to turn the tables? *Mol Cell Proteomics* **12**, 2381-2382, (2013).

78 Fingert, J. H., Stone, E. M., Sheffield, V. C. & Alward, W. L. Myocilin glaucoma. *Survey of ophthalmology* **47**, 547-561, (2002).

79 Yang, Y. F., Sun, Y. Y., Peters, D. M. & Keller, K. E. The Effects of Mechanical Stretch on Integrins and Filopodial-Associated Proteins in Normal and Glaucomatous Trabecular Meshwork Cells. *Front Cell Dev Biol* **10**, 886706, (2022).

80 Wilmarth, P. A., Riviere, M. A. & David, L. L. Techniques for accurate protein identification in shotgun proteomic studies of human, mouse, bovine, and chicken lenses. *J Ocul Biol Dis Infor* **2**, 223-234, (2009).

81 Chambers, M. C. *et al.* A cross-platform toolkit for mass spectrometry and proteomics. *Nat Biotechnol* **30**, 918-920, (2012).

82 Eng, J. K., Jahan, T. A. & Hoopmann, M. R. Comet: an open-source MS/MS sequence database search tool. *Proteomics* **13**, 22-24, (2013).

83 Keller, A., Nesvizhskii, A. I., Kolker, E. & Aebersold, R. Empirical statistical model to estimate the accuracy of peptide identifications made by MS/MS and database search. *Anal Chem* **74**, 5383-5392, (2002).

84 Robinson, M. D., McCarthy, D. J. & Smyth, G. K. edgeR: a Bioconductor package for differential expression analysis of digital gene expression data. *Bioinformatics* **26**, 139-140, (2010).
85 Robinson, M. D. & Oshlack, A. A scaling normalization method for differential expression analysis of RNA-seq data. *Genome Biol* **11**, R25, (2010).
86 Ge, S. X., Jung, D. & Yao, R. ShinyGO: a graphical gene-set enrichment tool for animals and plants. *Bioinformatics* **36**, 2628-2629, (2020).
87 Szklarczyk, D. *et al.* The STRING database in 2023: protein-protein association networks and functional enrichment analyses for any sequenced genome of interest. *Nucleic Acids Res* **51**, D638-D646, (2023).
88 Deutsch, E. W. *et al.* The ProteomeXchange consortium at 10 years: 2023 update. *Nucleic Acids Res* **51**, D1539-D1548, (2023).

**Figure 1**



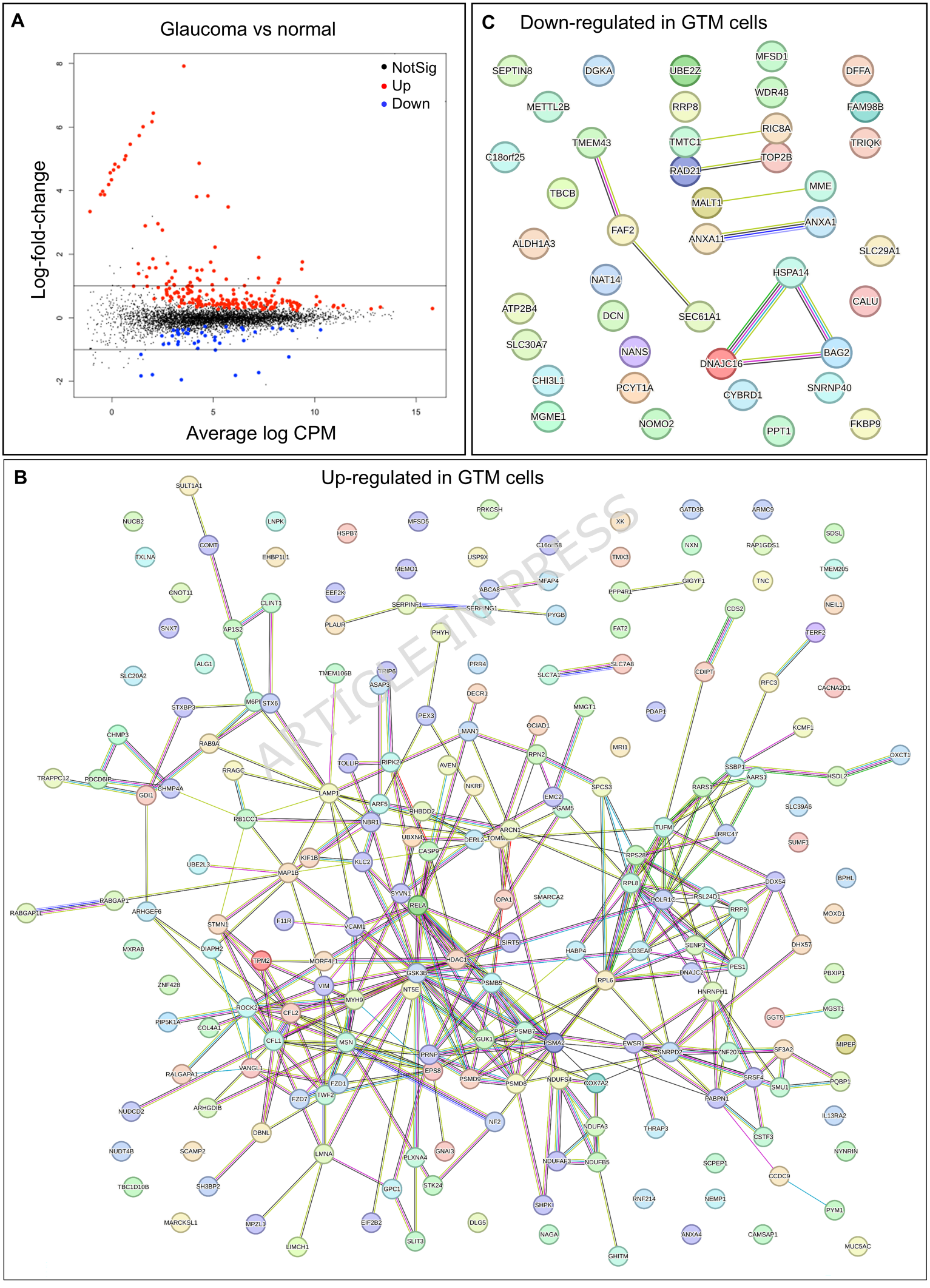

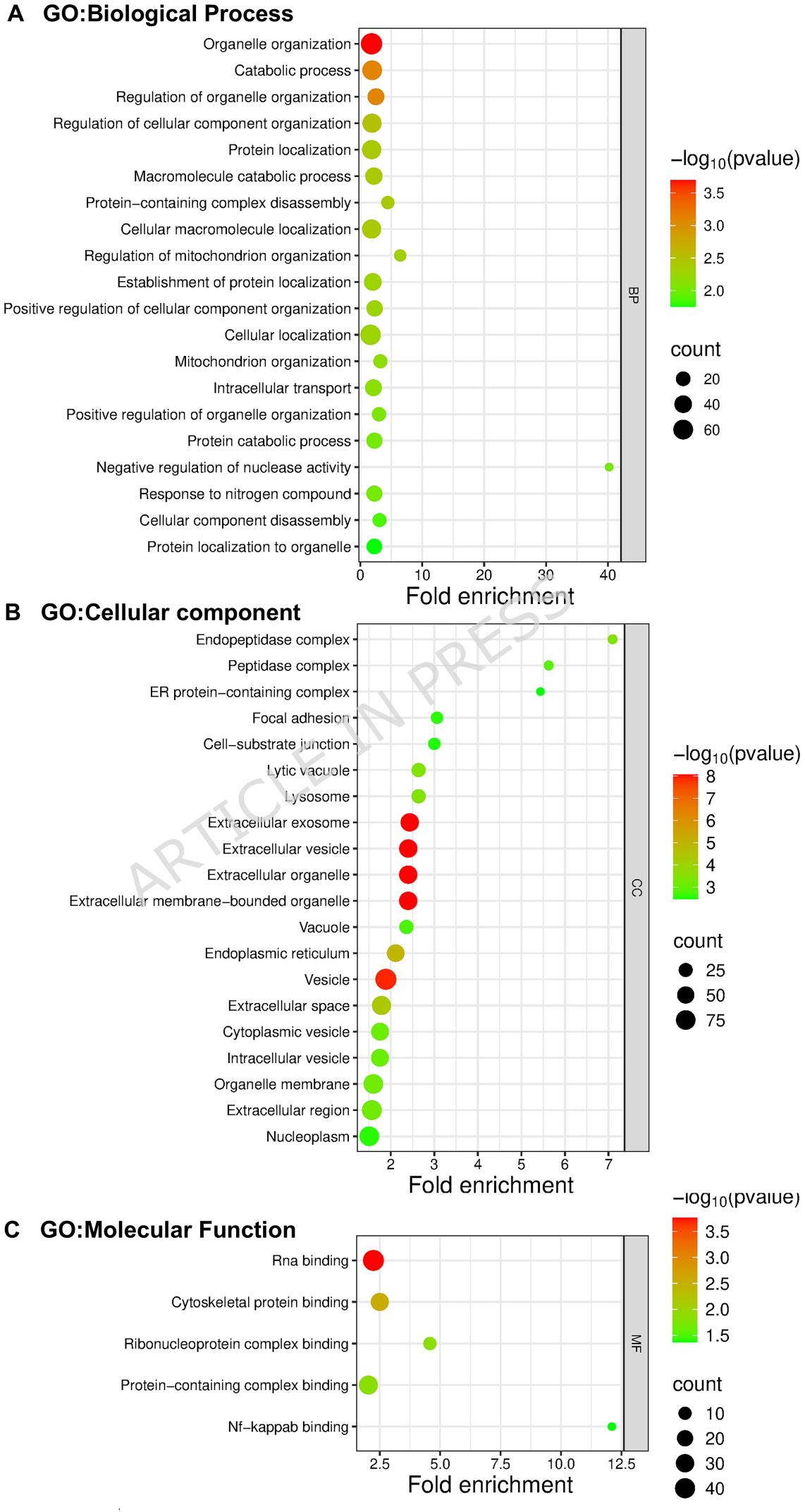

## Figure 3

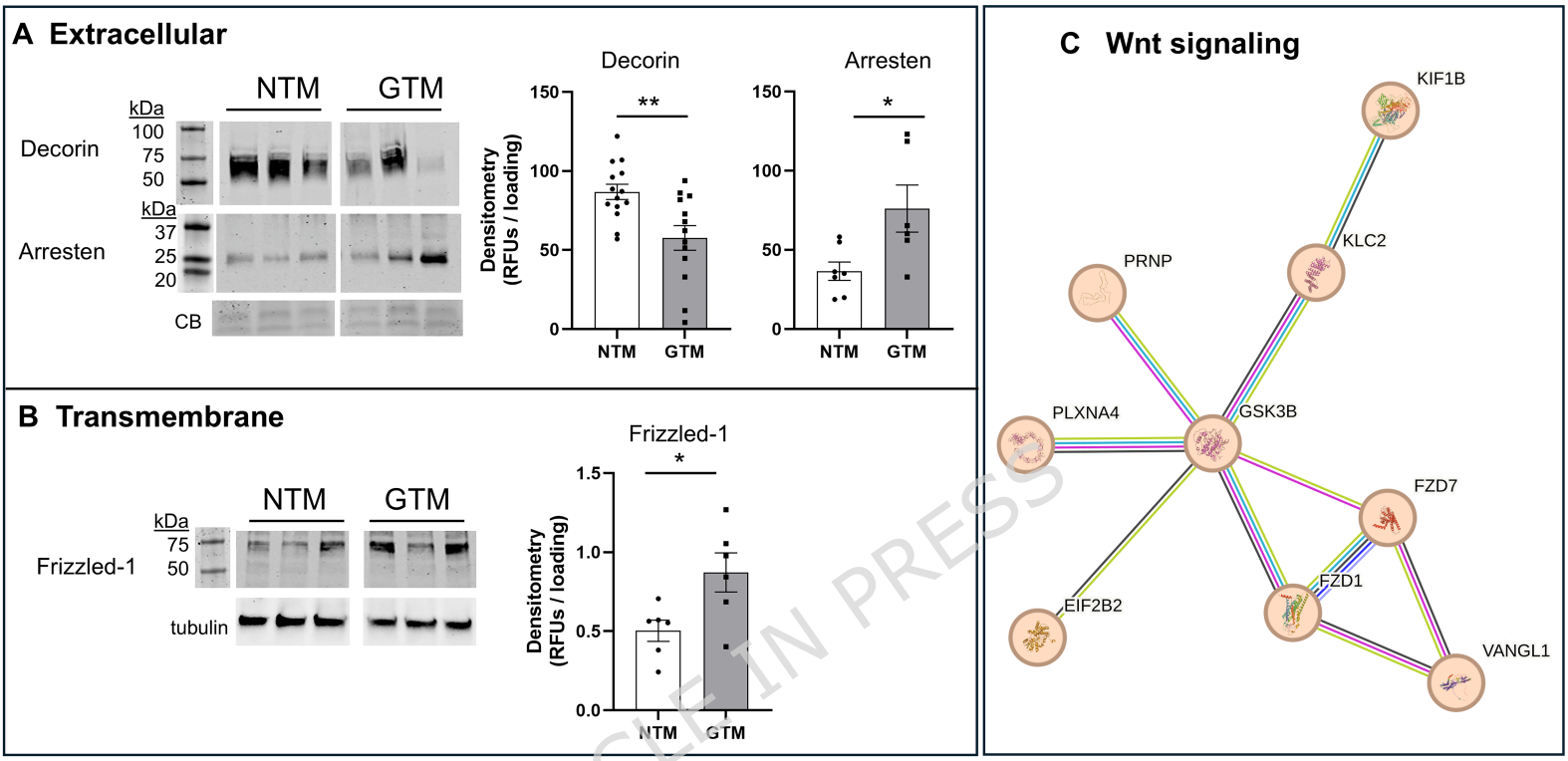

## Figure 4

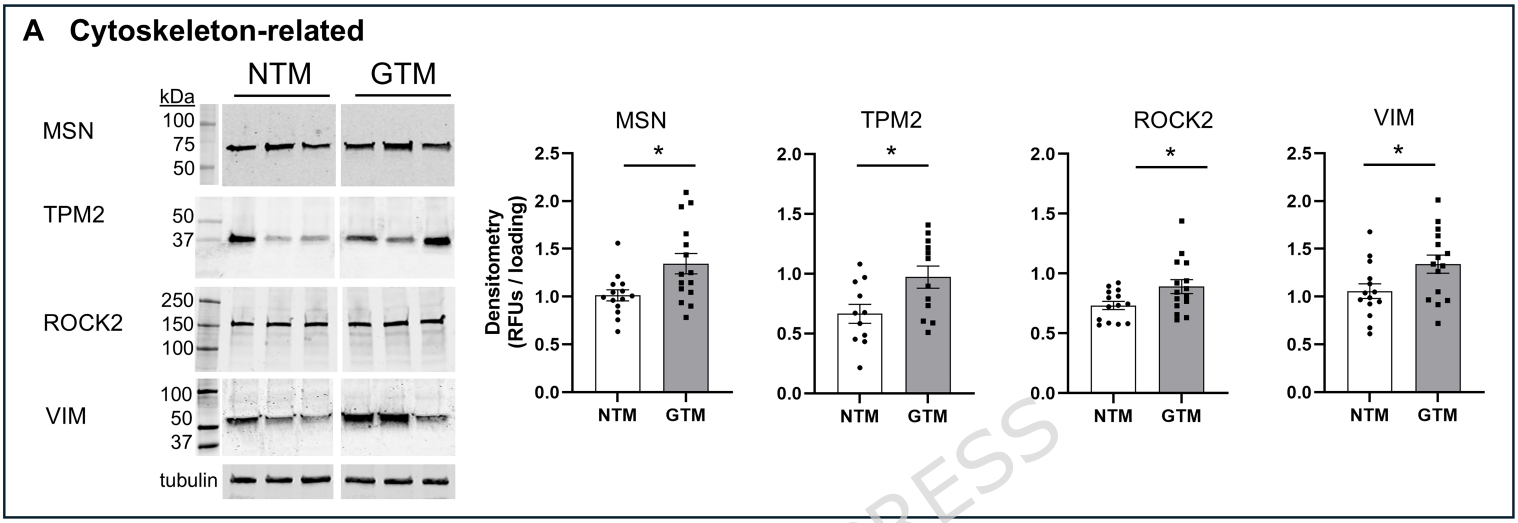


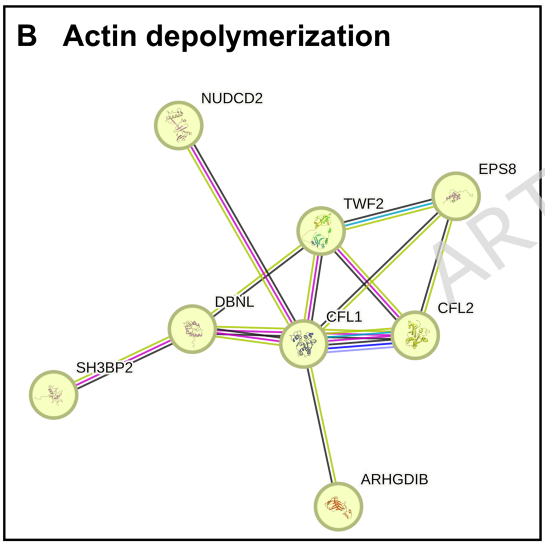


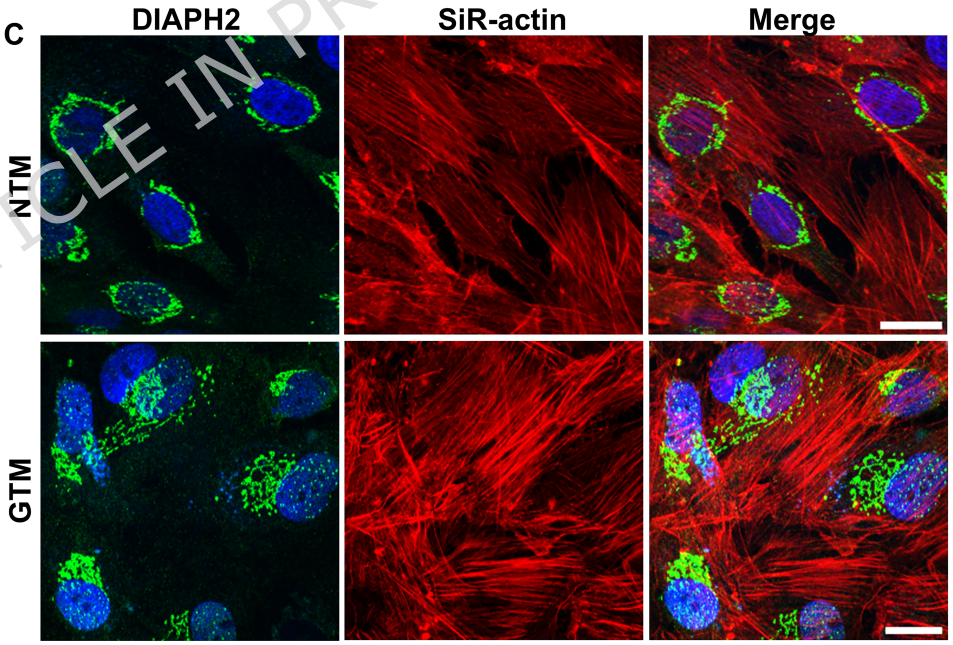

# Figure 5

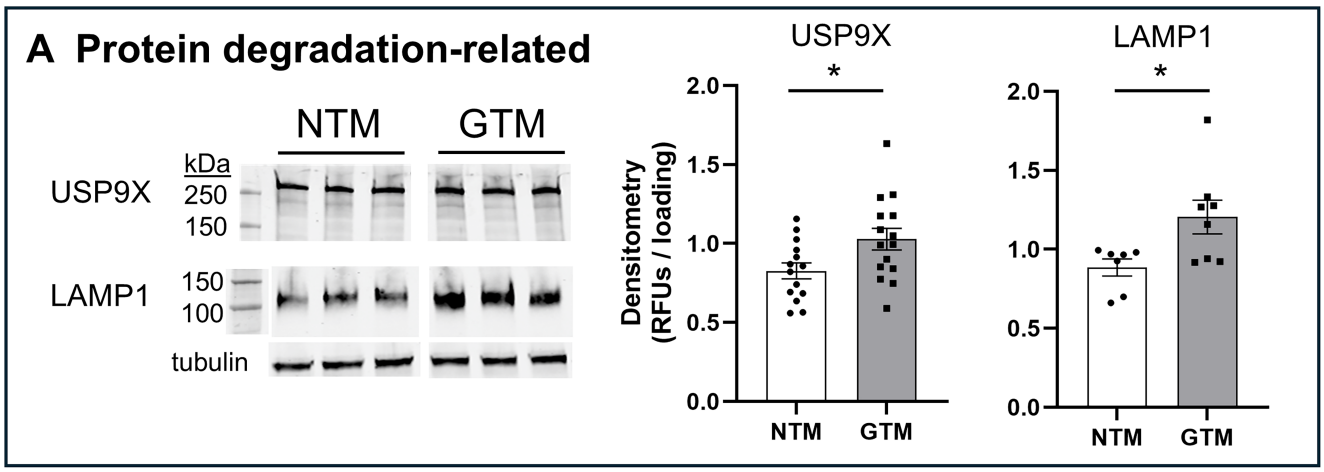


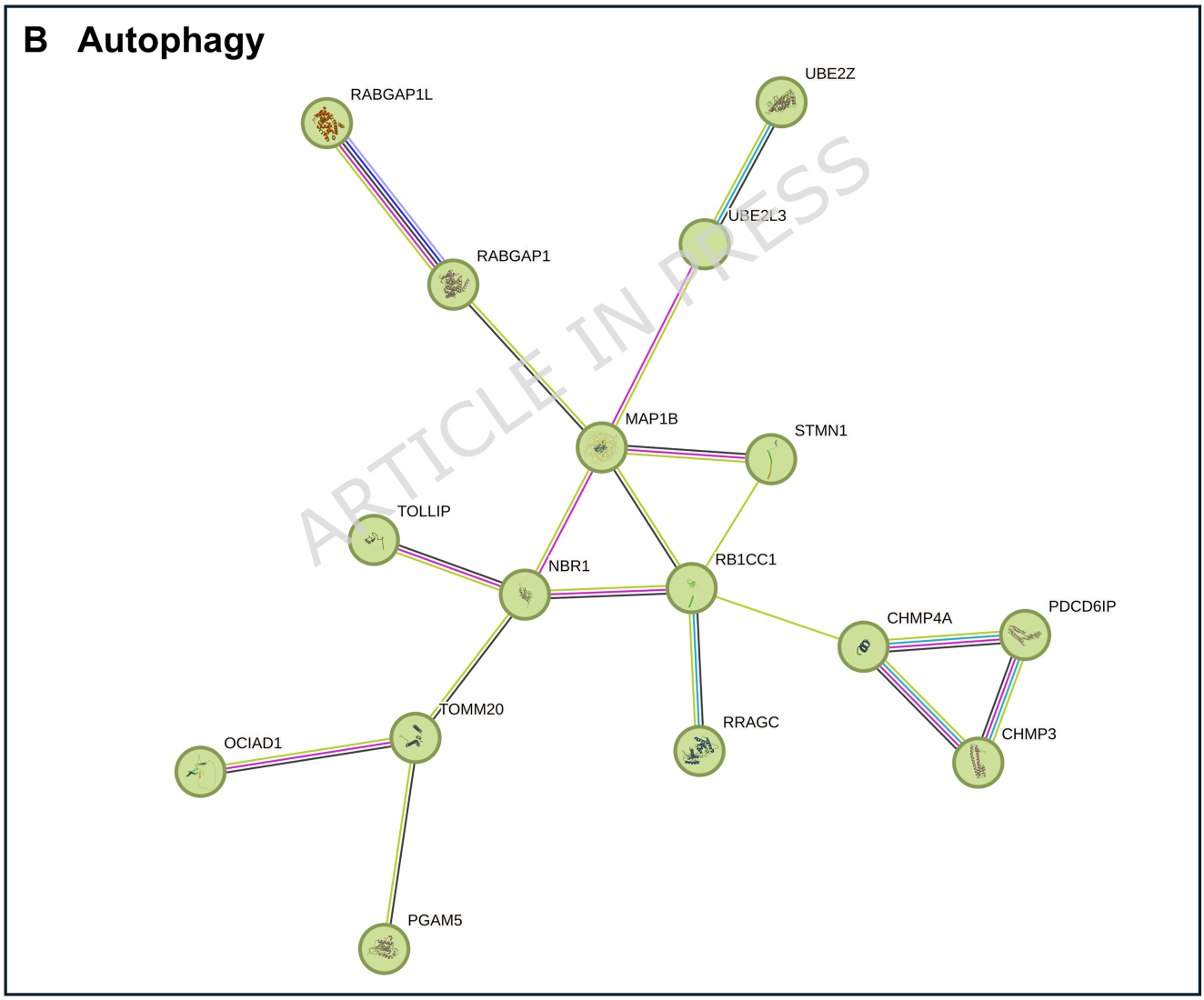

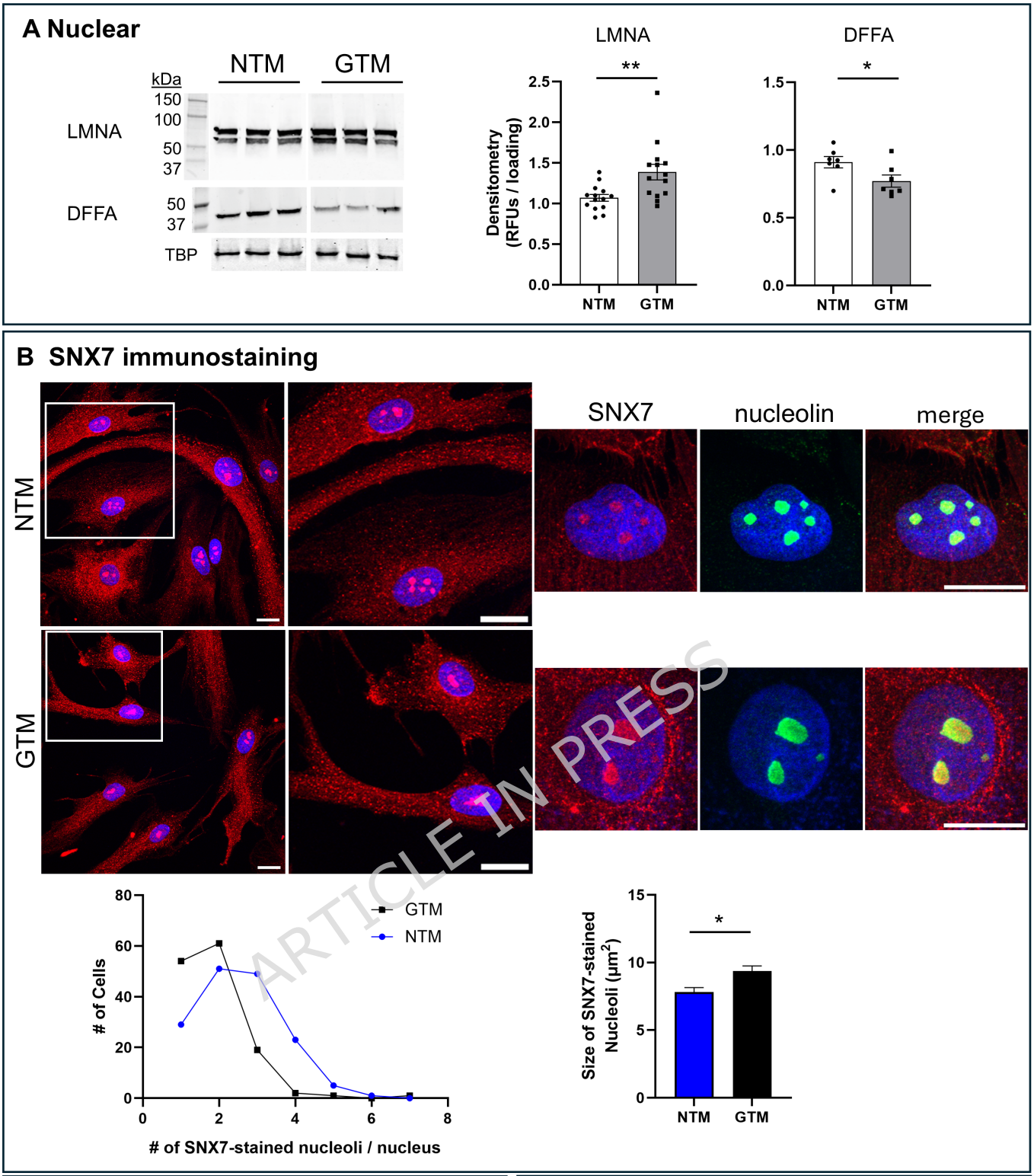

# Figure 7

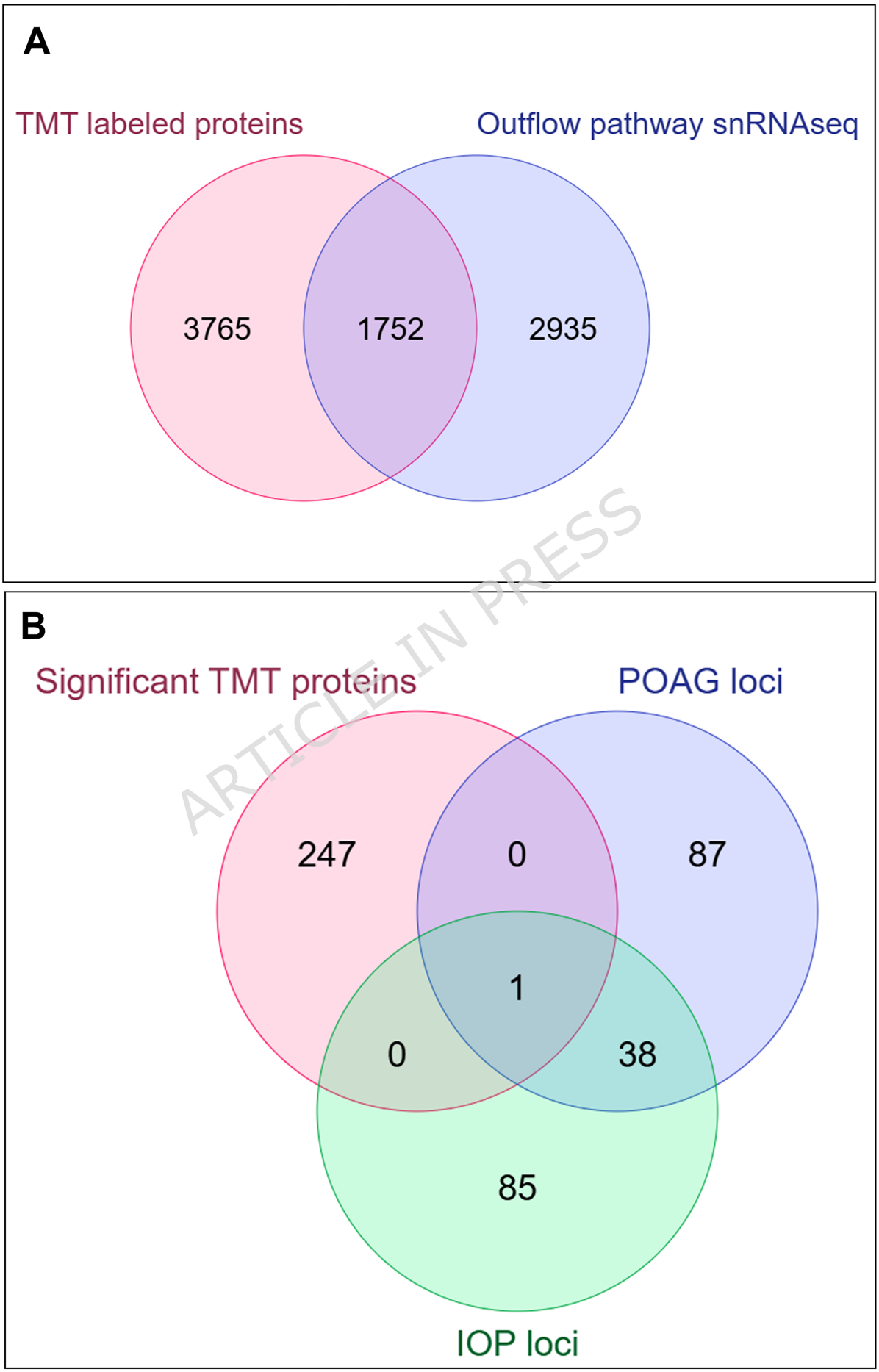

**Table 1. Demographics of human donor eyes used in this study**. Glaucoma status is shown, as well as medications (if known). POAG = primary open-angle glaucoma. Cell strains were used for TMTpro proteomics (TMT), Western immunoblot (WB), and/or immunofluorescence (IF) assays.

| Cell strain | Age | Sex | Cause of Death | Glaucoma (medication) | Experiment | Sample key |
|---|---|---|---|---|---|---|
| 2021-1493 | 74 | F | Subdural bleed | No | TMT; WB | N-wt-12 |
| 2022-0794 | 80 | M | Respiratory failure | No | TMT; WB | N-wt-1 |
| 2022-0140 | 77 | F | Cardiogenic shock | No | TMT; WB | N-hom-2 |
| 2022-0791 | 59 | M | Mantle cell lymphoma | No | TMT; WB | N-hom-6 |
| 2022-1032 | 71 | F | Natural causes | No | TMT; WB | N-wt-16 |
| 2020-0984 | 69 | M | Advanced Parkinson’s and dementia | No | IF | n/a |
| 2021-1110 | 77 | F | Lung cancer | No | WB; IF | n/a |
| 2022-0707 | 78 | F | Respiratory failure | No | WB; IF | n/a |
| 2023-0775 | 86 | M | Vfib arrest | No | WB | n/a |
| 2023-0747 | 76 | M | Natural causes | No | WB | n/a |
| | | | | | | |
| 2019-1757 | 92 | F | Cardiogenic shock | POAG (latanoprost) | TMT; WB | G-wt-9 |
| 2022-0949 | 61 | F | Pneumonia | POAG | TMT; WB | G-wt-17 |
| 2022-1033 | 78 | M | Cardiac arrest | POAG | TMT; WB | G-wt-15 |
| 2018-1672 | 57 | M | Respiratory failure | Glaucoma | TMT; WB | G-wt-5 |
| 2019-1150 | 81 | F | Breast cancer | POAG (combigan) | TMT; WB | G-hom-13 |
| 2021-0034 | 70 | M | Heart failure | POAG | WB | n/a |
| 2021-1912 | 73 | F | Myocardial infarction | Glaucoma | IF | n/a |
| 2022-1058 | 93 | F | Acute respiratory failure | Glaucoma | IF | n/a |

| | | | | | | |
|---|---|---|---|---|---|---|
| 2024-1471 | 81 | M | Cardiac arrest | Glaucoma | WB | n/a |
| 2024-1491 | 82 | M | Intracerebral hemorrhage | Glaucoma | WB | n/a |

**Table 2:** Top 20 up- and down-regulated (gray) differentially abundant proteins in GTM cells compared to NTM cells (FDR<0.1). LogFC is the log fold-change, FDR is the false discovery rate.

| Protein Name | Accession | Fold Change (FC) | logFC | P-value | FDR |
|---|---|---|---|---|---|
| CNOT11 | Q9UKZ1 | 241.969 | 7.918 | 0.000002 | 0.000363 |
| SNX7 | Q9UNH6 | 86.862 | 6.440 | 0.000002 | 0.000408 |
| CAMSAP1 | Q5T5Y3 | 71.950 | 6.168 | 0.000014 | 0.001330 |
| AVEN | Q9NQS1 | 64.520 | 6.011 | 0.000001 | 0.000288 |
| LMNA | P02545 | 53.160 | 5.731 | 0.000003 | 0.000456 |
| USP9X | Q93008 | 44.015 | 5.459 | 0.000001 | 0.000229 |
| ROCK2 | O75116 | 34.171 | 5.094 | 0.000002 | 0.000408 |
| PBXIP1 | Q96AQ6 | 31.610 | 4.981 | 0.000004 | 0.000514 |
| CCDC9 | Q9Y3X0 | 29.044 | 4.860 | 0.000005 | 0.000615 |
| SF3A2 | Q15428 | 28.482 | 4.831 | 0.000000 | 0.000101 |
| PYM1 | Q9BRP8 | 26.879 | 4.747 | 0.000002 | 0.000362 |
| STK24 | Q9Y6E0 | 25.130 | 4.650 | 0.000002 | 0.000362 |
| SHPK | Q9UHJ6 | 23.622 | 4.561 | 0.000032 | 0.002631 |
| DERL2 | Q9GZP9 | 20.282 | 4.341 | 0.000003 | 0.000484 |
| SH3BP2 | P78314 | 18.274 | 4.191 | 0.000004 | 0.000496 |
| MSN | P26038 | 15.760 | 3.977 | 0.000001 | 0.000267 |
| TPM2 | P07951 | 14.710 | 3.878 | 0.000007 | 0.000807 |
| TERF2 | Q15554 | 14.657 | 3.872 | 0.000013 | 0.001273 |
| MMGT1 | Q8N4V1 | 14.245 | 3.832 | 0.000003 | 0.000462 |
| RFC3 | P40938 | 14.024 | 3.810 | 0.000001 | 0.000288 |
| ANXA1 | P04083 | -1.483 | -0.568 | 0.002491 | 0.065476 |
| RRP8 | O43159 | -1.525 | -0.609 | 0.000142 | 0.007441 |
| SEPTIN8 | Q92599 | -1.634 | -0.708 | 0.000162 | 0.008339 |
| HSPA14 | Q0VDF9 | -1.644 | -0.717 | 0.002926 | 0.073732 |
| MALT1 | Q9UDY8 | -1.670 | -0.740 | 0.000126 | 0.006852 |
| ATP2B4 | P23634 | -1.688 | -0.755 | 0.001017 | 0.034864 |
| NANS | Q9NR45 | -1.741 | -0.800 | 0.002434 | 0.064889 |
| TMTC1 | Q8IUR5 | -1.744 | -0.802 | 0.000414 | 0.017568 |
| MME | P08473 | -1.756 | -0.812 | 0.003155 | 0.078074 |
| SNRNP40 | Q96DI7 | -1.783 | -0.834 | 0.002326 | 0.062619 |
| FAF2 | Q96CS3 | -1.785 | -0.836 | 0.000853 | 0.030470 |
| SLC29A1 | Q99808 | -1.950 | -0.964 | 0.000183 | 0.009084 |
| SLC30A7 | Q8NEW0 | -2.021 | -1.015 | 0.000301 | 0.013727 |
| METTL2B | Q6P1Q9 | -2.225 | -1.154 | 0.000067 | 0.004400 |
| ANXA11 | P50995 | -2.345 | -1.230 | 0.000076 | 0.004766 |
| DNAJC16 | Q9Y2G8 | -3.304 | -1.724 | 0.004169 | 0.095972 |
| CALU | O43852 | -3.460 | -1.791 | 0.004284 | 0.096176 |
| CYBRD1 | Q53TN4 | -3.511 | -1.812 | 0.000001 | 0.000218 |
| SEC61A1 | P61619 | -3.550 | -1.828 | 0.002924 | 0.073732 |
| TBCB | Q99426 | -3.860 | -1.949 | 0.002301 | 0.062229 |